Chapter 14
Nanotechnology for Oil-Water Separation

Prakash M. Gore, Anukrishna Purushothaman, Minoo Naebe, Xungai Wang, and Balasubramanian Kandasubramanian

Contents

P. M. Gore
Nano Surface Texturing Lab, Department of Metallurgical & Materials Engineering, DIAT (DU), Ministry of Defence, Pune, Girinagar, India

Institute for Frontier Materials, Deakin University, Geelong, VIC, Australia

A. Purushothaman
Centre for Biopolymer Science and Technology, Central Institute of Plastics Engineering and Technology, Eloor, Udyogmandal, Kochi, India

M. Naebe · X. Wang
Institute for Frontier Materials, Deakin University, Geelong, VIC, Australia

B. Kandasubramanian (✉)
Nano Surface Texturing Lab, Department of Metallurgical & Materials Engineering, DIAT (DU), Ministry of Defence, Pune, Girinagar, India

R. Prasad, K. Thirugnanasambandham (eds.), *Advanced Research in Nanosciences for Water Technology*, Nanotechnology in the Life Sciences,
https://doi.org/10.1007/978-3-030-02381-2_14

14.1 Introduction

The increased consumption of oils and industrial solvents in recent decades for fulfilling the ever-increasing energy needs has accelerated the development of associated industries and world economies (Fingas 2012, 2015). The massive transportation of these oils and solvents to various industrial sectors is mainly accomplished via sea-based roots, which involves frequent oil-spills and accidents, e.g., Gulf of Mexico in 2011 (Fingas 2015; Hansen 2016). These oil seepages cause enormous amount of oils, i.e., ~1.7 to 8.8 million tons every year, being liberated in oceans, which accommodate highly sensitive marine ecosystem (Gore et al. 2016a; Gupta and Kandasubramanian 2017a). These oil-spills traumatize the marine organisms and ecosystems, and further cause chemical toxicity and oxygen and light deficiency, thus threatening their survival (Fingas 2012, 2015). Researchers have explored various chemical, biological, and physical techniques for accomplishing the effective oil-water separation for countering the oil-seepages in such situations. Recently, researchers have been exploring nanomaterials for efficient oil/solvent-water separation, as they render highly active surface area, improved functionality with ability to tailor the properties, and nano-scale dispersion (Xue et al. 2014; Arora and Balasubramanian 2014; Padaki et al. 2015; Yadav et al. 2016; Breitwieser et al. 2018; Simon et al. 2018; Walker et al. 2018; Padhi et al. 2018). The literature analysis done via Web of Science reveals nearly 868 articles being published in last 10 years, i.e., from year 2008 to 2018, on oil-water separation using nanomaterials, stating their rapidly increasing importance. Further, the literature analysis shows that the average number of research papers published on oil-water separation using nanomaterials have increased at an average rate of 145% (Fig. 14.1a).

Considering, the abovementioned techniques, the physical absorption method involves utilization of foams (Mishra and Balasubramanian 2014; Arora and Balasubramanian 2014), activated carbon (Ma et al. 2016), textiles substrates (Gore et al. 2016b), metal fine mesh (Matsubayashi et al. 2017), and fibers (Xue et al. 2014), which have been widely explored by the researchers.. The recently developed techniques such as electrospinning (Cheng et al. 2017; Gore and Kandasubramanian 2018), layer-by-layer assembly, selective oil extraction, and air-flotation have also gained wide attention by researchers for effective oil-water separation, due to their facile fabrication (Xue et al. 2014; Wang et al. 2015a; Ma et al. 2016). In order to achieve the efficient oil-water separation, the materials exhibiting high superwettability (Sahoo and Kandasubramanian 2014a; Sahoo and Balasubramanian 2014) absorption performance towards oil and/or water is required, which is mainly dependent on their surface characteristics such as superhydrophobicity/oleophobicity (water/oil contact angle $>150°$), superhydrophilicity/oleophilicity (water/oil contact angle $\sim 0°$), and hierarchical surface roughness at nano/-micro scale, thus making

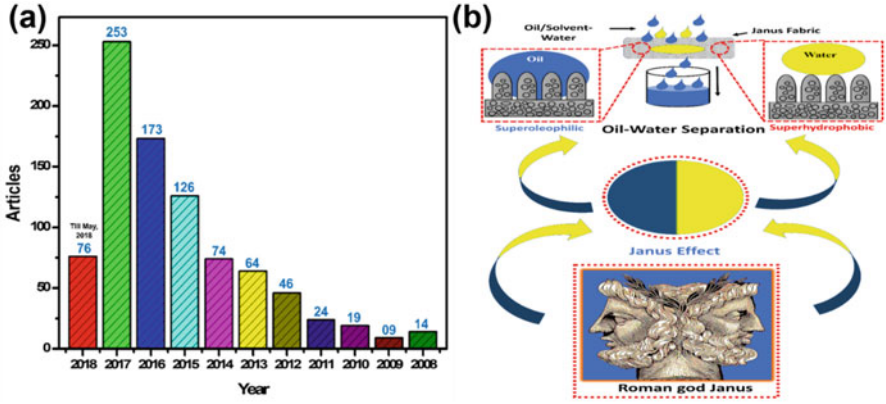

Fig. 14.1 (**a**) Scopus literature analysis, (**b**) Janus Effect, and its utilization in Oil-Water separation (Saini and Kandasubramanian 2018). (Reprinted with permission. Copyright 2018, Taylor and Francis)

them effective superwettable material (Xue et al. 2014). Various plants and animal surfaces manifest the superhydrophobicity with water contact angle (WCA) greater than 150° and sliding angle less than 10° which inspires the bionic creations having unique wettability structures, such as *Nelumbo nucifera* (Lotus) leaf surface (Sahoo and Kandasubramanian 2014b; Sahoo and Balasubramanian 2014; Sahoo et al. 2015). The liquids with lesser surface tension than the Lotus leaf show the immediate spreading and penetration of liquid. The surfaces with surface tension less than water (72.8 mN m^{-1}), greater than oil/organic solvents (<30 mN m^{-1}), exhibit the heterogeneous wettability towards the oil/organic solvents and water, simultaneously (Gupta et al. 2017).

The functionality and performance of the materials and methods can be enhanced for effective oil-water separation using nanomaterials via in situ mixing or via their respective synthesis routes, as they facilitate highly active surface area, improved functionality with ability to tailor the properties, and nano-scale dispersion (Xue et al. 2014; Ma et al. 2016). Recently, nano-functionalized superwetting materials like Janus fabrics, membranes, nanofibers, sponges, and foams have been explored for oil-water separation, and water-effluent treatment (Sahoo et al. 2013, 2014; Arora et al. 2014; Sahoo and Kandasubramanian 2014c; Bhalara et al. 2014, 2015; Rule et al. 2014; Hudlikar et al. 2014; Gonte et al. 2014; Banerjee and Balasubramanian 2015; Balasubramanian et al. 2015; Khanale and Balasubramanian 2016; Sharma et al. 2016; Khurana and Balasubramanian 2016; Gonte and Balasubramanian 2016; Gupta et al. 2016; Amal Raj et al. 2017; Gore et al. 2017, 2018a, b), as they render high separation efficiency, recyclability, mechanical robustness, and elevated performance under stringent environmental conditions (Mishra and Balasubramanian 2014; Arora and Balasubramanian 2014; Gore et al. 2016b; Gore and Kandasubramanian 2018). These superwetting nano-engineered materials are potential candidates for treating oil/solvent-water mixture/emulsions in large quantities.

14.2 Superwettable Janus Materials

The working concept of these materials has stemmed from the unique "Janus particles," where half of its part acts as a hydrophobic and other half part acts as a hydrophilic, thus bringing dual characteristics in same particles (Walther and Müller 2008, 2013). The term "Janus" to these particles was coined by the researchers, by correlating its characteristics to the Roman god Janus, who possesses two reverse faces (opposite to each other), portraying the future and past (Gore et al. 2016b; Gupta and Kandasubramanian 2017a; Gore and Kandasubramanian 2018) (Fig. 14.1b). The researchers have used this concept for the preparation of the Janus materials for oil-water separation, where at least half of the part of the material exhibits either superhydrophobicity/oleophobicity or superhydrophilicity/oleophilicity and vice versa.

In one of the studies, Gore and Kandasubramanian have fabricated the Janus fabric engineered with cotton, and polylactic acid (PLA) microfibers, decorated with surface-modified nanoclay (NC) (montmorillonite base) (Gore and Kandasubramanian 2018). The developed Janus fabric prepared using electrospinning method demonstrated superhydrophobicity, i.e., WCA ~ 152°, superhydrophilicity, i.e., WCA ~ 0°, and superoleophilicity, i.e., OCA ~ 0° (Fig. 14.2a–c) Further, their Janus fabric demonstrated oil-water separation efficiency of 99.16% (Fig. 14.2f), till 30 washing cycles, with a maximum permeation flux of ~65,000 $L \cdot m^{-2} \cdot h^{-1}$ for n-hexane solvent from solvent-water mixture (Fig. 14.2e).

They claimed that the superhydrophobicity in the Janus fabric was achieved using the nano/-micro scale hierarchical rough structure, and the observed intrinsic porosity in the generated PLA/NC microfibers, which is further supported by the FESEM analysis (Fig. 14.2d). Further, they reported that the inherent hydrophobicity of PLA microfibers was enhanced under the influence of surface functionalized (amine engineered) nanoclay exhibiting montmorillonite base, bringing the superhydrophobic attribute to the PLA/NC microfibers (Gore and Kandasubramanian 2018).

Furthermore, the developed Janus fabric revealed biodegradation under in-house arranged biotic decompost slurry setup, via microbial and hydrolytic conditions (Fig. 14.3b). The biodegradation analysis revealed a 78% weight loss at a rate of $2.79 \pm 0.5\%$ per day (at room temperature), in 28 days. Their biodegradation results were confirmed by the wetting analysis, weight loss analysis, and morphological analysis (Fig. 14.3a).

Further the morphological analysis of the degraded Janus fabric samples showed the existence of Gram-positive *Bacillus polymyxa* bacteria. Additionally, the developed Janus fabric sustained harsh chemical environments such as subzero temperatures (−20 to 0 °C), hypersaline solutions (10 to 30%), acidic and basic (pH = 1 to 10), and mild-detergent solution, UV-radiation (254 nm) (Gore and Kandasubramanian 2018).

In another study, our group showed a fabrication of a hydrophobic/oleophilic Janus fabric based on Polyvinylidene Fluoride (PVDF) and nano Silicon Carbide (nano-SiC) (5 wt%) via electrospinning technique (Fig. 14.4a) (Gore et al. 2016a).

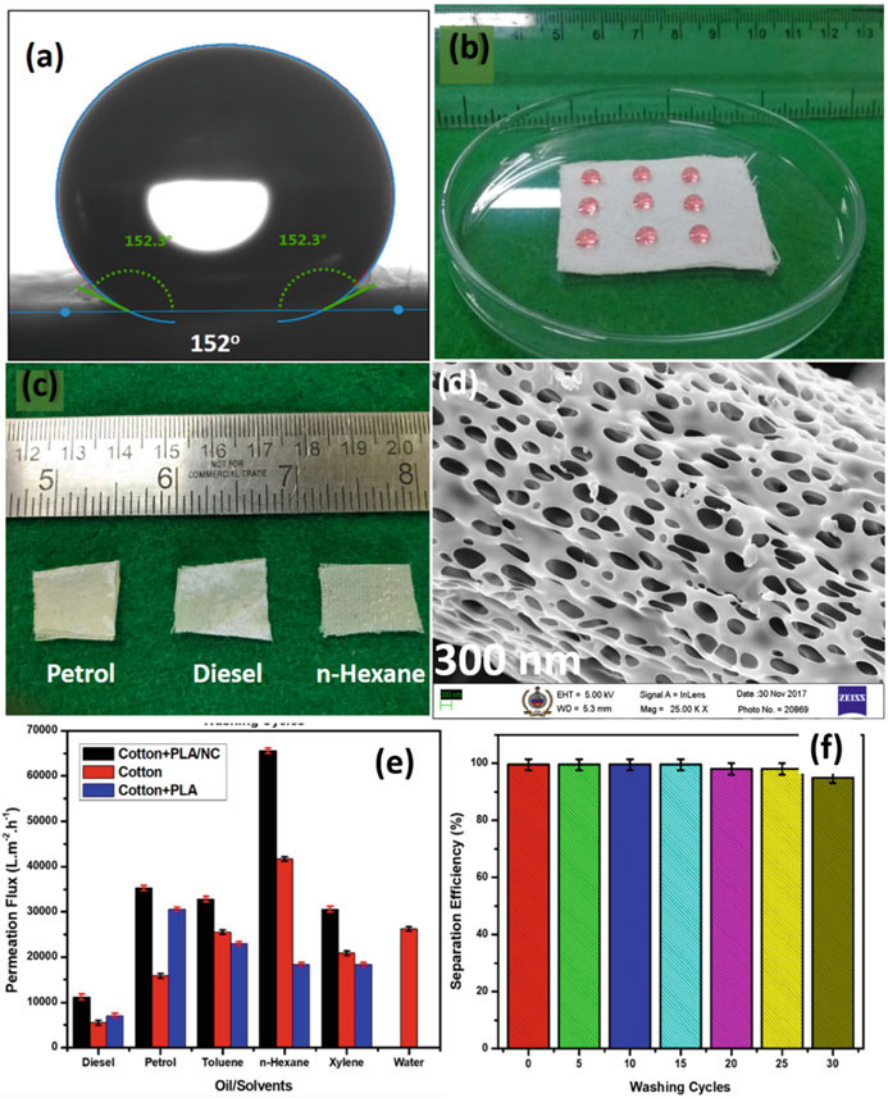

Fig. 14.2 (**a**) WCA of Janus fabric, (**b**) Superhydrophobicity in Janus fabric, (**c**) Superoleophilicity in Janus fabric, (**d**) FESEM analysis of Janus fabric at 300 nm, (**e**) Permeation flux, (**f**) Separation efficiency with respect to washing cycles (Gore and Kandasubramanian 2018). (Reprinted with permission. Copyright 2018, Royal Society of Chemistry)

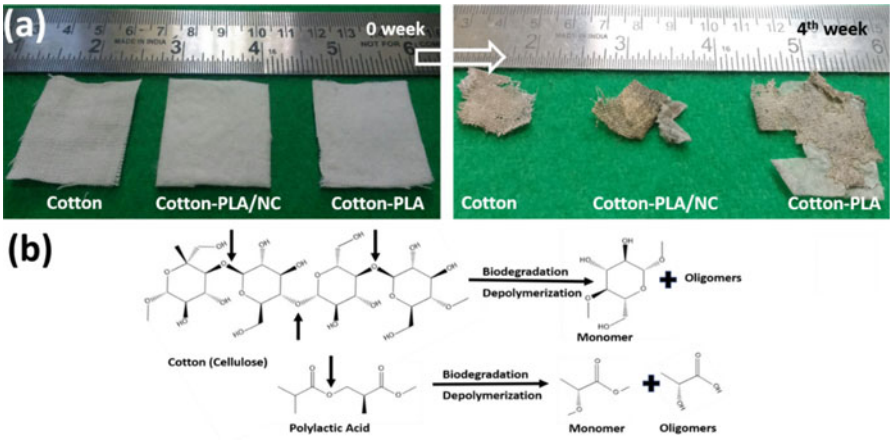

Fig. 14.3 (**a**) Biodegradation of Janus fabric samples, (**b**) proposed biodegradation mechanism (Gore and Kandasubramanian 2018). (Reprinted with permission. Copyright 2018, Royal Society of Chemistry)

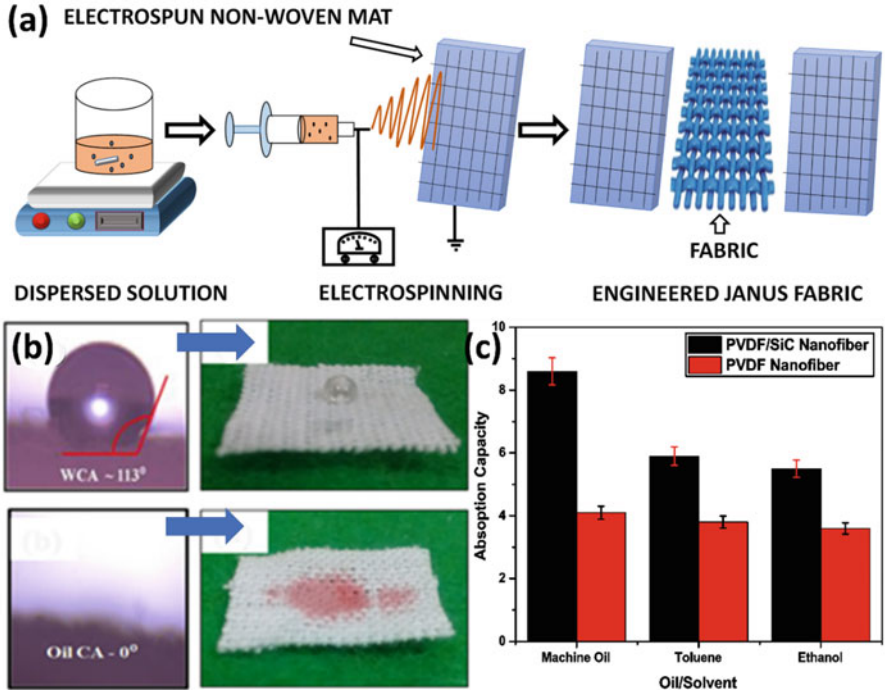

Fig. 14.4 (**a**) Electrospinning of Janus fabric, (**b**) Hydrophobicity, and superoleophilicity in Janus fabric, (**c**) Absorption performance of Janus fabric for oils and solvents (Gore et al. 2016a). (Reprinted with permission. Copyright 2016, Royal Society of Chemistry)

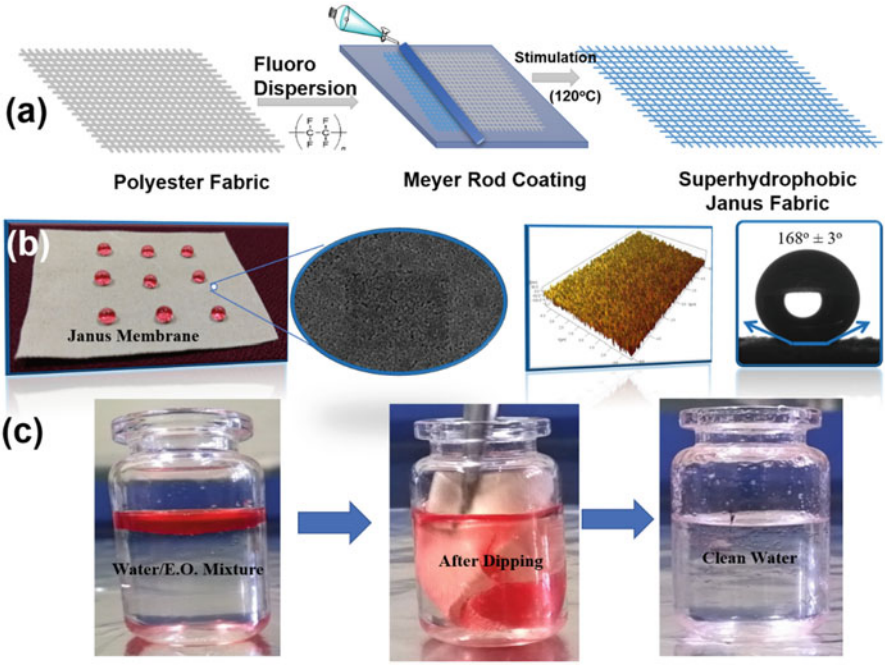

Fig. 14.5 (**a**) Janus membrane fabrication, (**b**) Superhydrophobicity, FESEM, AFM, and contact angle analysis, (**c**) Practical oil-water-separation performance (Gupta and Kandasubramanian 2017a). (Reprinted with permission. Copyright 2017, American Chemical Society)

The PVDF/nano-SiC nanofibers were electrospun onto the cotton fabric surface, which showed a maximum hydrophobicity, i.e., WCA ~ 113°, and superoleophilicity, i.e., OCA ~ 0° (Fig. 14.4b). Morphological and air permeability analysis demonstrated the influence of the randomly networked porous nanofibers enhancing the hydrophobicity of the Janus fabric. The developed Janus fabric effectively separated the oil and solvent from mixture with absorption capacities up to 8.6, 5.9, and 5.5 times the Machine oil, Toluene, and Ethanol, respectively, which can further be recycled till 10 cycles (Fig. 14.4c) (Gore et al. 2016a).

Recently, Gupta and Kandasubramanian have developed a Janus membrane based on Cotton fabric and nano-dispersion of PTFE polymer, fabricated via Meyer-Rod coating method (Fig. 14.5a) (Gupta and Kandasubramanian 2017a). The developed Janus membrane exhibited a Janus effect with a superhydrophobicity (WCA ~ 168°)/superoleophilicity (OCA ~ 0°) (Fig. 14.5b), along with an oil-water separation efficiency of 98% (Fig. 14.5c) coupled with retainment of characteristic properties till 30 washing cycles. Further, their Janus membrane also showed flame retardation and ice-phobic characteristics, with resistance to hypersaline (Brine) solution (10% to 30%), UV-resistance to light with 254 nm wavelength, high thermal stability at a temperature of 150 to −20 °C (subzero temperature) (Gupta and Kandasubramanian 2017a).

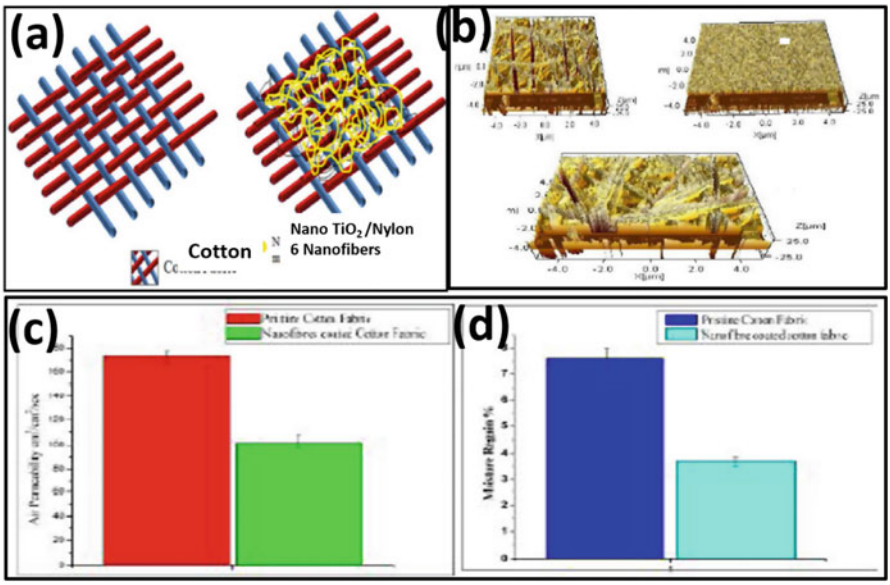

Fig. 14.6 (**a**) Nylon-6/TiO_2 Nanofiber membrane fabrication, (**b**) AFM Analysis, (**c**) Air permeability analysis, (**d**) Unidirectional Water absorption (**c**) (Dhanshetty and Balasubramanian 2016)

Sahoo et al. have reported that hydrophobic property can be added on to the surface via surface roughness, or by changing the surface chemistry with materials exhibiting intrinsic hydrophobicity (Sahoo and Kandasubramanian 2014b; Sahoo and Balasubramanian 2014; Sahoo et al. 2015). With further approach, researchers have utilized nanoparticles (NP) with intrinsic hydrophobicity like TiO_2 (Shi et al. 2016), ZnO (Tian et al. 2012a), and SiO_2 (Wu et al. 2015), for making the superhydrophobic materials based on electrospinning.

Dhanshetty and Kandasubramanian have developed hydrophobic Janus Fabric via electrospinning (Fig. 14.6a), using Nylon-6 polymer and TiO_2 nanoparticles ($\leq$200 nm), which exhibited unidirectional transport property for water. Their developed Janus fabric based on Nylon-6/TiO_2 showed hydrophobicity (WCA ~ 99.7°)/hydrophilicity (WCA ~ 30.86°), i.e., Janus effect, simultaneously, and average surface roughness of around 106 nm (Fig. 14.6b). Further, the FT-IR analysis revealed characteristics peaks 807 and 1021 cm^{-1} for TiO_2 nanoparticles, whereas the FESEM analysis revealed hierarchical morphology exhibiting pores with entangled networked morphology of Nylon-6/TiO_2 nanofibers, responsible for the hydrophobic nature, along with unidirectional water absorption × air permeability (Fig. 14.6c, d) (Dhanshetty and Balasubramanian 2016).

In other study, Simon and Kandasubramanian have fabricated a nanofibrous membrane based on nano/micro-scaled carbon (camphor) soot (CS) particles (3 wt %) and fluoroelastomer via electrospinning method (Simon and Kandasubramanian 2018). The developed membrane exhibited a hydrophobic (WCA ~ 143°) and oleophilic (OCA ~ 0°) characteristics with hierarchical porous morphology. They

claimed that the 3 wt% loading of carbon soot particles in Fluoroelastomers helped in elevating the hydrophobicity of the matrix, i.e., from WCA ~ 128° to WCA ~ 143°, and the dispersion of soot particles further enhanced the mechanical strength of the nanofibrous membrane. The developed CS based membrane revealed an absorption capacity of 1.1 times and 2.6 times of its weight for Diesel and Engine Oil, respectively, whereas the pristine Fluoroelastomer membrane revealed absorption capacity of 1.5 time and 4.3 times of its weight for Diesel and Engine oil, respectively. The decrease in the absorption capacity of CS engineered nanofibrous membrane was attributed to the blocking of the pores due to the high dispersion of CS particles in the nanofibrous membrane. The FT-IR analysis of the Fluoro/CS nanofibrous membrane revealed characteristic peak at 882, 1143, and 1386 cm^{-1} which were attributed to vinylidene group, —C—F—, and —C—F_2 bond stretch vibrations of vinylidene difluoride (VDF) and hexafluoropropylene (HFP) functional groups present in the fluoroelastomer. The stress-strain analysis of the membranes revealed a tensile stress of 360 and 310 N/mm^2 for the CS engineered nanofibrous membrane and pristine fluoro nanofibrous membrane. Their developed Fluoro/CS nanofibrous membrane further revealed an anti-icing property, where it effectively removed the frozen water droplets from the surface of the membrane in 4 s, under an applied airstream pressure of 100 kPa. Further, the fabricated Fluoro/CS nanofibrous membrane demonstrated petal effect for water droplets, which they rendered it to impregnated Cassie-wetting regime, which was also supported by the anti-icing characterization (Simon and Kandasubramanian 2018).

14.3 Superwettable Janus Membrane Based on Polycarbonate and Nano-Copper Phthalocyanine

The oil-seepage accidents generally involve severe working conditions in sea-based environments, where the utilized superwettable materials need high separation efficiency, along with chemical and mechanical robustness. In this sense, our group had developed thermally and mechanically stable superhydrophobic Janus membrane based on engineering thermoplastic of Polycarbonate (PC), and nano-Copper Phthalocyanine (CuPc) particles. PC being an engineering thermoplastic exhibits high mechanical stability (tensile modulus ~ 62 MPa) and thermal stability (glass transition ~ 147 °C) (Brydson 1999; Lin et al. 2016), and the nano-CuPc is (blue color) a pigment in solid powder form, which exhibits thermal stability up to a temperature of 480 °C, along with high chemical resistance (for acids & alkalis) (Moser and Thomas 1964; Schwieger et al. 2002; Hunger 2002; Jiang 2010). The Janus microfiber membrane was developed using facile electrospinning, which demonstrated superhydrophobicity with a water contact angle of 158 ± 2°, and superoleophilicity with oil contact angle of 0°. Further, the Janus microfiber membrane revealed oil-water separation efficiency of 97%, along with a high permeation flux of 6903 and 5802 $L{\cdot}m^{-2}{\cdot}h^{-1}$, respectively, for Petrol and Diesel. The Janus

microfiber membrane further demonstrated a theoretical capillary pressures of −9833 and −9670 N/m^2, respectively, for Diesel and Petrol, revealing its affinity towards oils. The developed microfiber membrane also showed a theoretical breakthrough pressure of 1.260 kPa, which demonstrated its resistance to cross-flow of water. The successive results demonstrate that the developed Janus microfiber membrane can be effectively used for emphatic oil-water separation during oil-seepage catastrophes.

The homogenous solution for electrospinning operation was prepared by dissolving Polycarbonate (PC) in Chloroform solvent at a concentration of 25 wt/v % using magnetic hot plate stirrer, where the solution was allowed to stir for 3 h at room temperature. Further, the Copper Phthalocyanine (CuPc) was added in individual PC solutions, as 0.5, 1, 1.5, 2, 3, and 5wt/wt%, respectively, and the solution was stirred at high rpm (~800) for 10–15 min. Then, the developed homogenous solutions of pristine Polycarbonate and Polycarbonate/Copper Phthalocyanine were used for further electrospinning operation.

The fabrication of PC/CuPc Nanofibers was performed in a horizontal electrospinning unit (ESPIN-Nano, India) at an applied voltage of 17 kV using a 10 mL syringe fitted with a metal needle (diameter ~ 0.55 mm) (Fig. 14.4a). The distance between the needle and the collector plate was maintained at 12 cm. The flow/feed rate for both pristine Polycarbonate and polycarbonate-Copper Phthalocyanine solutions was maintained at 1.5 mL/h. The electrospun nanofibers were collected in a non-woven form, and were subsequently dried at a temperature of 70° for ensuring the complete removal of the solvent phase.

In order to establish the Janus microfibers as an efficient material for oil-water separation, its oil-water separation performance has been investigated experimentally. The electrospun Janus microfibers were characterized for petroleum products such as diesel and petrol, along with organic solvent. The electrospun samples of Janus microfibers (diameter ~ 4.5 cm) were placed in the channel assembly of the separation device. The freshly prepared oil-water mixture in 1:1 ratio was poured on to the Janus microfiber membrane, under the action of gravitational force. The experiment was repeated and average separation efficiency of consecutive estimations was calculated. The separation efficiency was calculated via following equation (Gore and Kandasubramanian 2018):

$$\text{Separation efficiency} = \frac{V_2}{V_1} \times 100 \tag{14.1}$$

where, V_1 and V_2 = Volume of oil, before and after separation.

Permeation flux was calculated via following equation (Gore and Kandasubramanian 2018):

$$J = \frac{V}{A \times t} \tag{14.2}$$

where J = Permeation flux (L·m^{-2}·h^{-1}).

V = Volume of oil (L).
A = Surface area of the membrane (m).
t = Time (h).

14.4 Results and Discussion

FT-IR analysis was performed for pristine polycarbonate (PC), Copper Phthalocyanine (CuPc) powder, and PC/CuPc (2wt/wt%) nanofibers (Fig. 14.7a) for determining the present functional groups in the electrospun microfiber membrane. The FT-IR analysis of pristine polycarbonate shows major peaks at 1767 cm^{-1} which is attributed to carbonyl peak generated by oxygen atoms double bonded to carbon atom, peak at 1506 cm^{-1} is assigned to the phenol ring stretching, at this peak the resonance frequency of two phenol ring is reached, the peak at 1220 cm^{-1} corresponds to asymmetric O—C—O carbonate stretching, 1188 cm^{-1} peak is assigned to C—O bond deformation and last peak at 837 cm^{-1} assigned to the existence of para substituted phenol rings in the back bone of the polycarbonate (Dybal et al. 1998; Parshin et al. 2013; Ghorbel et al. 2014).

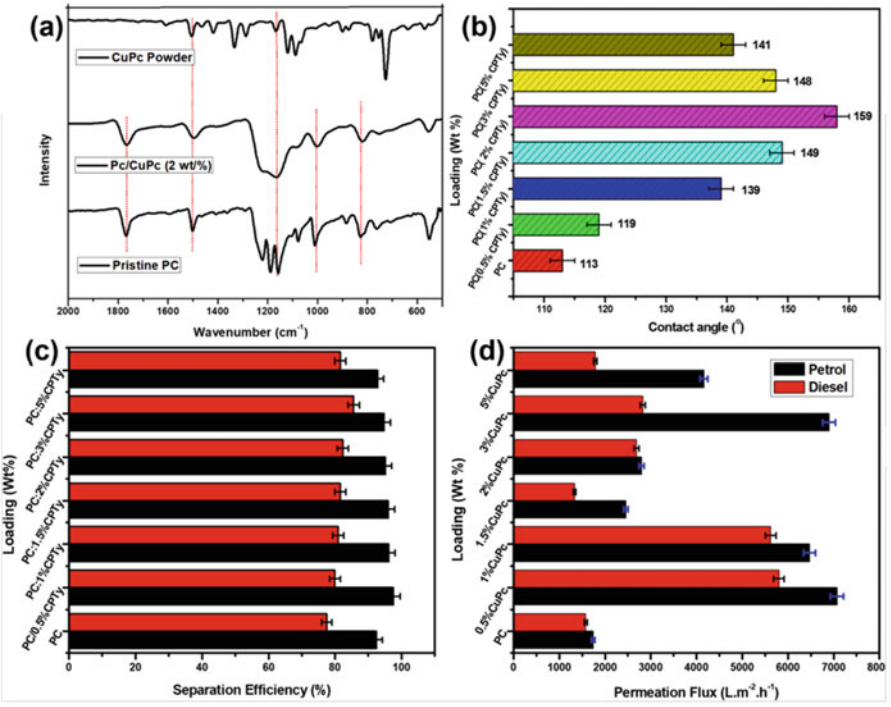

Fig. 14.7 (**a**) FTIR spectrum of pristine PC, CuPC Powder, and PC/CuPC Nanofibers (2wt/wt%), (**b**) Contact angle analysis, (**c**) Separation performance, and (**d**) Permeation flux analysis

The FT-IR study of Copper Phthalocyanine (CuPc) shows small peak at 1607 cm^{-1} which is assigned to the benzene C—C stretching, the peak at 1505 cm^{-1} is possibly due to the pyrrole deformation, the peaks at 1464 and 1418 cm^{-1} were assigned to the iso indole stretching, the peak at 1334 cm^{-1} is most probably the pyrrole C—C stretching coupled with aza rocking, 1287 cm^{-1}, the peaks at 1167, 1119, 1088 and 754 cm^{-1} were assigned to the common pyrrole C—C stretching, C—H deformation, iso indole deformation, pyrrole C—N asymmetric and Pc ring deformation, respectively (Fig. 14.7a). FTIR spectrum of PC/CuPc microfibers shows characteristic peaks of both polycarbonate and copper phthalocyanine with decreased stretching C—O bond, slight variations are observed at other characteristic peaks 2906, 1765, 1495, 1165, 819, 752, and 552 cm^{-1}. The disappeared peaks of CuPc at 754 and 1334 cm^{-1} imply that the CuPc has well mixed and dispersed in PC/CuPc system (Fig. 14.7a) (Schwieger et al. 2002; Seoudi et al. 2005; Salzman et al. 2005; Georgiev et al. 2008; Padma et al. 2009).

14.4.1 Morphological Analysis

The morphological study of the nanofibers was performed using FESEM analysis. The FESEM micrograph of pristine PC microfibers (Fig. 14.8a) demonstrates heterogeneous rough surface and intrinsic porous morphology along with an average fiber diameter of ~2.1 μm. Figure 14.8b reveals microfibers of PC/2CPTy at 2 wt% loading with randomly ordered nanopores, whereas Fig. 14.8c reveals its microfiber at 300 nm scale at 20 kX magnification. Further, from Fig. 14.8c, it is observed that, the number of pores are less in PC/2CPTy microfibers having 2 wt% loading, as compared to pristine PC microfibers, which could be attributed to the uniform distribution of Copper Phthalocyanine nanoparticles. The average diameter of the observed pores is around 140 nm. Figure 14.8d depicts the FESEM micrograph of Copper Phthalocyanine (CuPc) taken at 300 nm range with 50 kX magnification. Figure 14.8d shows that the CuPc exhibits clustered morphology in its solid form, having an average cluster diameter of 2.3 μm. The clusters are formed of CuPc nanoparticles, which exhibit average nanoparticle diameter in the range from 102 to 152 nm. During the preparation of the electrospinning solution, these clusters get disintegrated into the individual nanoparticles under the action of mechanical stirring, and further gets uniformly distributed into the PC matrix, as revealed from the Fig. 14.8a–c.

The generation of the nanopores in the developed microfibers is attributed to that of the chloroform ($CHCl_3$) solvent, which evaporates out in the air, when the generated microfiber travels from needle-tip to collector plate. The stretched microfiber possesses increased surface area, which further facilitates the fast evaporation of the chloroform molecules. After the electrospinning operation, the collected microfibers are kept in air-oven for drying at a temperature of 70 °C for about 2 h, which helps in complete removal of chloroform solvent. The complete removal chloroform solvent is ensured at this stage, since it possesses a boiling point of

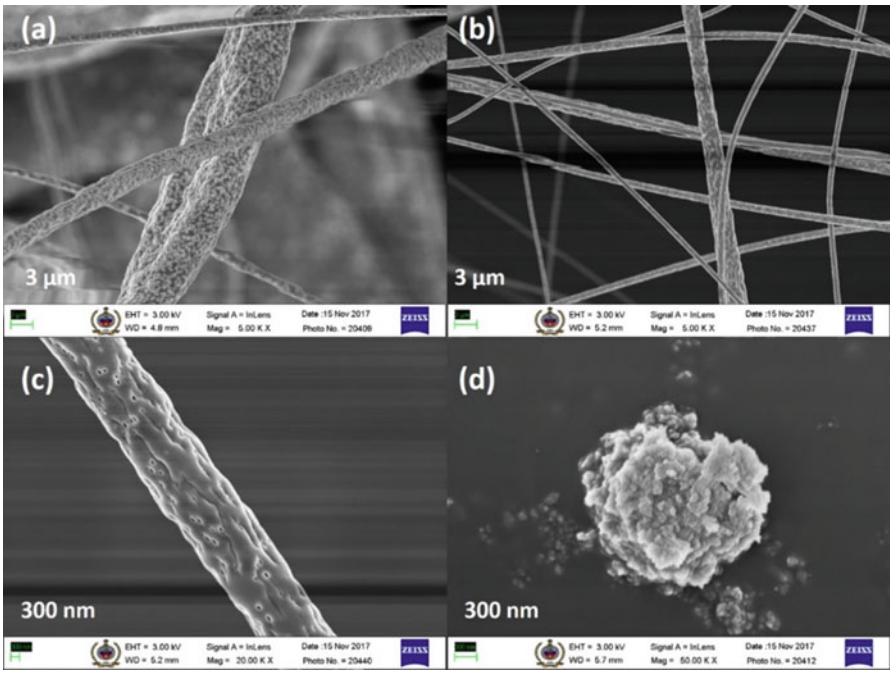

Fig. 14.8 (**a**) FE-SEM micrographs (**a**) Pristine Polycarbonate (PC) Nanofibers, (**b**) Polycarbonate/Copper Phthalocyanine PC/(2 CPTy) Nanofibers at 2 wt% loading, (**c**) PC/(2 CPTy) Nanofibers at 2 wt% loading (300 nm), (**d**) Copper Phthalocyanine Nanoparticles (300 nm)

around ~61 °C, which is less than drying temperature, i.e., 70 °C, of microfibers. The chloroform solvent creates space in the form of nanopores, which facilitates its easy removal during its evaporation. The generation of porous morphology is essentially required in the microfibers for the development of rough heterogeneous hierarchical surface texture, when superhydrophobicity-oleophilicity is necessarily required in the material (Mishra and Balasubramanian 2014; Arora and Balasubramanian 2014; Gupta and Kandasubramanian 2017a; Gore and Kandasubramanian 2018).

The wettability study of the developed Janus microfibers was performed experimentally via static contact angle method via Young-Laplace fitting method on contact angle goniometer (DSA 25, Kruss GmbH) for water, organic solvents, and petroleum oils. The fluid droplets of standard volume of 8 µL were placed on the surface of the Pristine PC and Janus microfibers, and the resulting contact angles were measured using goniometer. The PC/CuPC Janus microfibrous surface displays Lotus effect when the water droplet deposited on the surface of fibrous material.

The contact angles were found to vary with loading of the Copper Phthalocyanine (CuPc) in Polycarbonate (PC) as shown in Fig. 14.12. The pristine PC microfibers revealed a WCA of ~113°, thus showing its intrinsic hydrophobic nature, which could be attributed to the rough surface morphology, and generated nanopores

(diameter ~ 140 nm), and the polar groups, i.e., —CO and —COO, present in the polymer chain of the PC. Further, the results show that the WCA of the Janus microfibers has increased with the progressive loading of Copper Phthalocyanine (CuPc) from 0.5 wt% till 2 wt%, i.e., 119° to 158° (Fig. 14.7b). The further loading of CuPc from 3 wt% to 5 wt% decreased the WCA of the Janus microfibers, i.e., 148° to 141° (Fig. 14.7b), which shows that the maximum observed percolation is at 2 wt%. It can also be concluded that the 2 wt% loading facilitates the uniform distribution of the CuPc in the PC matrix, and the polar —CN groups further helps in elevating the hydrophobicity of the Janus microfibers to superhydrophobicity, which is supported by the respective FE-SEM and WCA analysis in Figs. 14.7a and 14.8. The contact angles of petroleum oils and solvents for pristine PC and Janus microfibers were found to be 0°, which demonstrates its superoleophilic nature. The petroleum oils readily wetted the Janus microfibers with an instant absorption of the droplets. Thus, the developed microfibers exhibited the selective wettability towards water, organic solvent, and petroleum oils.

The hydrophobicity of Pristine PC microfibers, with homogeneous rough surface, can be demonstrated via Wenzel's theory, which depicts the roughness of the surface as main driving factor for the generation of the hydrophobic attributes in the substrate. This phenomenon is explained using Wenzel's principle equation as (Wenzel 1936; Gupta and Kandasubramanian 2017a; Gore and Kandasubramanian 2018):

$$\cos\theta_w = r\frac{(\gamma_{sv} - \gamma_{sl})}{\gamma_{lv}} = r\cos\theta \tag{14.3}$$

where θ_w = surface water contact angle,

θ = Young's contact angle,

r = the surface roughness factor, i.e., the ratio of authentic and projected surface area.

Wenzel's equation explains the hydrophobic behavior of homogeneous rough surfaces; however, it does not explain the hydrophobicity in heterogeneous rough surfaces. The developed Janus microfibers possesses heterogeneous rough surface, along with inherent nanopores (Fig. 14.8) due to the presence of CuPc (Kamo and Kurosawa 1992; Rezaeifard et al. 2012). The generation of nanopores in Janus microfibers facilitate the creation of air-pockets between pores and rough textured surface, which restricts the permeation of water through the microfibers. In the present study, the hydrophobicity in the pristine PC microfibers, i.e., 113°, is elevated to superhydrophobicity, i.e., 158°, in Janus microfibers, is fundamentally explained using Cassie-Baxter Theory (Mishra and Balasubramanian 2014; Sahoo and Kandasubramanian 2014b; Sahoo and Balasubramanian 2014; Gupta and Kandasubramanian 2017a; Gore and Kandasubramanian 2018). Cassie-Baxter's theory well explains the superhydrophobic behavior of the substrates exhibiting heterogeneous rough surfaces possessing pores, via following principle equation

(Cassie and Baxter 1944; Sahoo and Kandasubramanian 2014b; Gore and Kandasubramanian 2018):

$$\cos\ \theta_c = f_1 \cos\ \theta_1 - f_2 \tag{14.4}$$

where θ_c = apparent contact angle,

f_1 & f_2= surface fractions of phase 1 and phase 2 respectively,

θ_1 = contact angle on phase 1.

Considering the heterogeneous porous Janus microfibers (as revealed in FESEM analysis), the randomly arranged 3D network of fibers, the surface roughness, and the intrinsic hydrophobic nature of PC polymer have aided in bringing the superhydrophobic attributes. The low surface energy of substrates is also a paramount factor responsible for generating the superhydrophobicity for water, in the present study the presence of CuPc could be the main driving factor for decreasing the surface energy of Janus microfibers. The superhydrophobicity (158°) present in the developed Janus microfibers is also attributed to the increased surface tension (γ) of water, i.e., γ_{water} ~ 72.8 mN/m, whereas the superoleophilicity (OCA ~ 0°) is attributed to the lower surface tension of petroleum oils, i.e., Petrol (γ_{petrol} ~ 29 mN/m) and Diesel (γ_{Diesel} ~ 29.5 mN/m). It is also found that the incremental addition of copper phthalocyanine (CuPc) has successively improved the water contact angle from 113 ± 2° to 158 ± 2° (Fig. 14.7b) (Kamo and Kurosawa 1992; Rezaeifard et al. 2012; Arora and Balasubramanian 2014; Gore et al. 2016a; Gupta and Kandasubramanian 2017a).

Considering the abovementioned results, aided with the superhydrophobic and superoleophilic attributes, the developed Janus microfibers demonstrate selective wettability, where it allows only petroleum oils and solvent to pass through its cross-sectional surface area, and restricts the entry of water, thus demonstrating its practical applicability for oil-water separation.

In order to establish the Janus microfibers as efficient material for oil-water separation, its oil-water separation performance needs to be evaluated.

During the oil-water separation experiments, the oil-water or solvent-water mixture (40 mL) was taken, which contained equal volume of oil-water or solvent, i.e., 20 mL each. Subsequently, the Janus microfiber membrane was treated with oil-water mixture, where it allowed only oil and solvent to pass through its active cross-sectional area (due to oleophilicity), and recovered the water on the membrane surface (due to superhydrophobicity). The amount of volume oil or solvent, before and after the analysis were taken, and the respective separation efficiencies of Janus microfiber membrane with various loadings of CuPC were calculated using previously mentioned Eq. (14.1). The practical separation efficiencies observed for Janus microfiber membranes have been shown in Fig. 14.7c.

It is was observed that the Janus microfiber membrane containing 0.5 wt% loading of CuPC demonstrated maximum separation efficiency of 97.6%, whereas the membrane with 5 wt% loading of CuPc demonstrated separation efficiency of 93.6%. The separation efficiency for Petrol was found to be higher as compared to Diesel, which is attributed to its lower viscosity as compared to Diesel (Fig. 14.7c).

The separation performance of Janus microfiber membrane is also associated with the difference in surface tensions of water, oil, and solvent (Gore et al. 2016a; Gupta and Kandasubramanian 2017), the hydrophobic nature, lower surface energy, and acting capillary forces, which synergistically improve the performance of Janus microfiber membrane. The observed nanopores in the Janus microfibers and the manifesting voids between them facilitate the storing space for the oils and solvents, and further allows the liquids to be transported to the opposite side of the membrane (Xue et al. 2014; Ma et al. 2016).

The time taken by Janus microfiber membrane to complete single separation cycle was approximately 20 min, which contains 10 min of drying in heating oven at a temperature of 70 °C, followed by 10 min for oil-water separation, and finally 5 min for cleaning of the membrane in ethanol-water mixture.

14.4.2 Separation Performance

The Oil-water separation performance of the Janus microfiber membrane was evaluated via permeation flux analysis. Figure 14.7d depicts the permeation flux performance of Janus microfiber membranes for petroleum oils. The results reveal that the petrol exhibits higher permeation flux, which could be attributed to its lower surface tension, i.e., 29 mN/m, as compared to Diesel, i.e., 29.5 mN/m (Gore et al. 2016a; Gupta and Kandasubramanian 2017; Gore and Kandasubramanian 2018). The Janus microfiber membrane with 0.5 wt% loading of CuPc has revealed a permeation flux of 7073 $L{\cdot}m^{-2}{\cdot}h^{1}$ for petrol and 5802 $L{\cdot}m^{-2}{\cdot}h^{-1}$ for diesel, whereas the membrane with 3 wt% loading of CuPc has revealed a permeation flux of 6903 $L{\cdot}m^{-2}{\cdot}h^{1}$ for petrol and 2829 $L{\cdot}m^{-2}{\cdot}h^{-1}$ for Diesel.

The lower permeation flux for Diesel is most likely due to its high viscosity as compared to other petrol, which generates a stronger adhesive forces with Janus microfiber membrane, thus increasing, i.e., delaying, its percolation time period. The observed visible differences in the permeation flux of petroleum oils could be associated to the variable factors such as viscosity, acting capillary forces, surface energy, and acting surface tensions, thereby directly influencing the performance of the membrane (Xue et al. 2014; Wang et al. 2015d; Ma et al. 2017; Gupta and Kandasubramanian 2017).

14.4.3 Capillary Pressure Study

Capillary action is a paramount driving factor, which is directly associated with the active capillary force, promoting the transport of liquids, i.e., oil and solvents, through the porous medium like Janus microfiber membrane. The Oil or water may diffuse evenly or accommodate onto the Janus microfiber membrane, which is attributed to its manifesting nanopores and surface wetting characteristic, i.e., superhydrophobicity-

superoleophilicity (Wang et al. 2015d; Gore and Kandasubramanian 2018). The superhydrophobic characteristic of the Janus microfibers holds the water onto its membrane surface, whereas the superoleophilicity helps in instant absorption and uniform distribution, i.e., spreading, of petroleum oils and solvents on the membrane surface, which is also confirmed by Gore and Kandasubramanian (2018). Further, Wang et al. have stated that the materials exhibiting porosity, e.g., Janus microfiber membrane, possess directional liquid-transport capability, which is more perplex in comparison with the materials possessing open, i.e., free, surfaces and filaments due to acting capillary stresses (Xue et al. 2014; Wang et al. 2015d; Ma et al. 2016). These forces get activated, when the fluid, i.e., oil or solvent, touches to the porous membrane. Homaeigohar et al. reported that the micro level pores manifesting in the porous materials show highly attractive capillary forces, in comparison to larger sized pores; thus, the micro level pores needs higher pressure to open-up (in the current study case, the required pressure for water to cross-through superhydrophobic surface) (Homaeigohar et al. 2010). Further, the superoleophilicity of the Janus microfibers membrane might get affected due to active capillary adhesive forces, get activated during the Oil/solvent-water separation. These manifesting active forces promote filling of the inter-voids occurring in the nano/-micro pores (Homaeigohar et al. 2010), thus maintaining continuous influx of oil-solvent through superhydrophobic-superoleophilic Janus microfiber membrane. The capillary pressure (P_{cap}) for a liquid, i.e., oil-solvent, passing through cylindrically shaped pore (in the present study, pores manifesting in the interconnected microfiber pores), is theoretically calculated via Young-Laplace's principle equation, as follows (Wang et al. 2015d; Gore and Kandasubramanian 2018):

$$P_{cap} = -\frac{2\gamma \mathrm{COS}\,\theta}{r} \tag{14.5}$$

where P_{cap} = Capillary pressure,
γ = Fluid surface tension,
r = Pore diameter, i.e., pores in interconnected microfiber,
θ = Contact angle of liquid on pore walls

When the surface of the membrane exhibits hydrophilic characteristic, i.e., $\theta < 90°$, then the positive capillary pressure generates, which transports the liquid into nano/-micro pores, and when the membrane surface exhibits hydrophobicity, i.e., $\theta > 90°$, then the negative pressure gets activated, where it restricts the entry of liquid in the pores.

In present study, the petroleum oils instantly wet the Janus microfiber membrane with even spreading; thus, the contact angle of the oils with pore wall can be presumed as 0°; hence, considering this, theoretical capillary pressures of petroleum oils for Janus microfiber membrane have been calculated, and are tabulated in Table 14.1. The capillary pressures of water could not be calculated for Pristine PC and Janus microfibers, due to limitation in analyzing the water contact angle with pore wall of inter-connected microfibers. The approximate average pore radius of interconnected microfibers of Pristine PC and Janus microfibers was found to be 20 μm and 6 μm, respectively (determined via FE-SEM analysis).

Table 14.1 Capillary pressures for various petroleum oils and organic solvents

Petroleum oils	Surface tension (mN/m)	Capillary pressure (N/m^2)	
		Pristine PC microfibers	Janus microfibers
Diesel	29.5	−2950	−9833
Petrol	29	−2900	−9670

Table 14.1 shows that the theoretically calculated capillary pressures for Janus microfibers are lower, i.e., −9833 and −9670 N/m^2 for Diesel and Petrol, respectively, which implies their maximum affinity towards oils, thereby facilitating the higher permeation of the oils through the Janus microfiber membrane. The theoretical capillary pressures for Pristine PC microfibers are found to be −2950 and −2900 N/m^2. The noticeable differences observed in the theoretically calculated capillary pressures is attributed to their pores radius, i.e., 20 μm for PC microfibers and 6 μm for Janus microfibers, which is related to the distance between the interconnected microfibers. Further, Table 14.1 also reveals that the capillary pressures decrease as the surface tension of oil decreases; this is attributed to the increased viscosity of oils, i.e., Diesel, having high surface tensions, which causes adhesion with Janus microfibers (Wang et al. 2015d; Yu et al. 2017b; Gore and Kandasubramanian 2018). This analysis is also reinforced by the lower permeation flux of Diesel, i.e., 6903 $L{\cdot}m^{-2}{\cdot}h^{-1}$ (for 3 wt% loaded CuPc), and the higher flux petrol, i.e., 2829 $L{\cdot}m^{-2}{\cdot}h^{-1}$ (for 3 wt% of CuPc).

14.4.4 Breakthrough Pressure Analysis

In order to prevent the failure of the Janus microfiber membrane due to cross-flow of water (which might occur under external force), hence, its breakthrough pressure analysis is important for determining its service performance.

Therefore, the breakthrough pressure can be calculated theoretically for Janus microfiber membrane by presuming the microfiber membrane as interconnected web with predominant cylindrically shaped structures (microfibers), via equation (Choi et al. 2009; Chhatre et al. 2010; Tian et al. 2012b; Gupta and Kandasubramanian 2017):

$$P_{\text{Breakthrough}} = \frac{l_{\text{cap}}(1 - \cos\theta)}{R\left(D^*_{\text{cylinder}} - 1\right)\left(D^*_{\text{cylinder}} - 1 + 2\sin\theta\right)} P_{\text{ref}} \tag{14.6}$$

where θ = contact angle between oil and microfiber membrane surface,

D^*_{cylinder} = estimation of porosity of surface porosity by presuming spacing and structure manifesting in the pores (dimensionless quantity), given by following equation (Choi et al. 2009; Chhatre et al. 2010; Tian et al. 2012b; Gupta and Kandasubramanian 2017):

$$D^*_{\text{cylinder}} = \frac{R + D}{R} \tag{14.7}$$

where R = radius of cylindrically shaped structures, i.e., microfibers, and
$2D$ = inter-cylinder spaces, i.e., inter-microfiber spaces.

P_{ref} is a least possible differential pressure for a liquid, i.e., oil, given by following equation (Chhatre et al. 2010):

$$P_{\text{ref}} = \frac{2\gamma}{l_{\text{cap}}} \tag{14.8}$$

where γ = surface tension,
l_{cap} = capillary length of liquid, calculated via following equation (Chhatre et al. 2010):

$$l_{\text{cap}} = \sqrt{\frac{\gamma}{\rho g}} \tag{14.9}$$

where ρ = liquid density,
g = acceleration due to gravity.

The Janus microfiber used in the present study revealed an approximate average diameter of 2.1 μm, and an average inter-cylinder (inter-microfiber) spacing of 6 μm (analyzed via FE-SEM and ImageJ application). The theoretically calculated breakthrough pressure for cross-flow of water through a surface of Janus microfiber (for WCA ~ 158°) membrane is found as 1.260 kPa, and for Pristine PC microfibers (for WCA ~ 113°) it is found to be 0.01978 kPa. The petroleum oils instantly get absorbed and transported via Janus microfiber membrane, which is also attributed to their varying surface tension, i.e., ($\gamma_{\text{water}} > \gamma_{\text{Janus microfiber membrane}} > \gamma_{\text{petroleum}-\text{oil}}$), and the water exhibiting high surface tension rest on membrane surface (Gupta and Kandasubramanian 2017).

Summary. In summary, superhydrophobic copper phthalocyanine pigmented nanofibers of polycarbonate were fabricated via electrospinning technique. The entrenched nanofibers exhibit an exceptional oil/water separation property. The pigmented fibrous material shows higher contact angle than the pristine electrospun membrane. The polycarbonate–copper phthalocyanine fibers possess high separation efficiency and high permeation flux (7073 $\text{Lm}^{-2}\ \text{h}^{-1}$) for petrol.

14.5 Superwettable Janus Fabric Based on Polyester and Nano-PTFE Particles

In our previously reported work, we described fabrication of Janus membrane using surfactant stabilized nano-PTFE dispersion onto cotton fabric via Meyer Rod coating technique, which demonstrated improved self-cleaning and anti-icing characteristic, flame-retardancy, water permeation breakthrough pressure, and comparable separation efficiency (Gupta and Kandasubramanian 2017a). The environmental catastrophes arising due to Oil-spill often involves harsh working condition, and hence the applied materials used during the oil-water separation need to be efficient, and mechanically robust during the service operations. Present study reports thermally stimulated superhydrophobic/oleophilic Janus fabric, exhibiting selective directional fluid gating effect for Oil-Water mixture, fabricated by impregnating nano-sized dispersion of Poly (1,1,2,2-tetrafluoroethylene) onto Poly (ethyl benzene-1,4-dicarboxylate) based fabric via scalable and automized padding technique. The engineered fabric exhibited superhydrophobicity-oleophilicity (WCA = 172° and OCA = 0°), low ice-adhesion, and self-cleaning characteristic which is attributed to its hierarchical surface texture having closely spaced randomly oriented nano-needle forest morphology generated on microfiber based fabric as revealed by FE-SEM micrograph. The as-prepared Janus fabric exhibited selective directional fluid gating with excellent separation efficiency up to 98% for various petroleum oils/solvents, with stable repeatability (till 30 recurrences), flame-retardancy, anti-icing characteristic, and a maximum permeation fluxes for n-Hexane, Toluene, and Petrol, i.e., 14597.65 $L{\cdot}m^{-2}{\cdot}h^{-1}$, 5016.87 $L{\cdot}m^{-2}{\cdot}h^{-1}$, and 7501.904 $L{\cdot}m^{-2}{\cdot}h^{-1}$, respectively, for Janus fabric. The reported Janus fabric also retained its intrinsic properties under extreme environmental conditions such as UV-irradiation (254 nm), hypersaline solution, extreme acidic and alkaline solutions (pH 1 and 14, respectively), high temperature (180 °C), and subzero temperature (−20 °C).

The commercial polyester fabric based on Poly (ethyl benzene-1,4-dicarboxylate) (plain weaved, 180 g/m^2, thickness = 190 μm, warp = 38/cm, weft = 38/cm) was procured from Ahmedabad Textile Industry's Research Association, India. Fluorosystem dispersion, i.e., Poly (1,1,2,2-tetrafluoroethylene), was acquired from the Chemours Company, India (Teflon™ PTFE DISP 33LX, PTFE content—61%, Density—1.52 g/cm^3, particle size ~ 0.220 μm, aided with wetting agent) (Chemours 2016).

The Janus fabric was fabricated using a stable fluorosystem dispersion onto the commercial Polyester fabric via padding technique (Fig. 14.9a). The padding rate and roller squeezing pressure were maintained at 1 m/min and 200 kN/m, respectively, to get the uniformity in coated fabric. For ensuring the complete penetration and deposition of dispersion inside the microfiber pores of the fabric, three padding cycles were carried out sequentially (Fig. 14.9a). The rotation of the squeezing rolls in the padding system creates tangential speed at the roller nips, due to which a drag force is generated on the dispersion in forward direction during coating on the fabric (Birley et al. 1992). The uniform distribution of pressure, i.e., 200 kN, from the

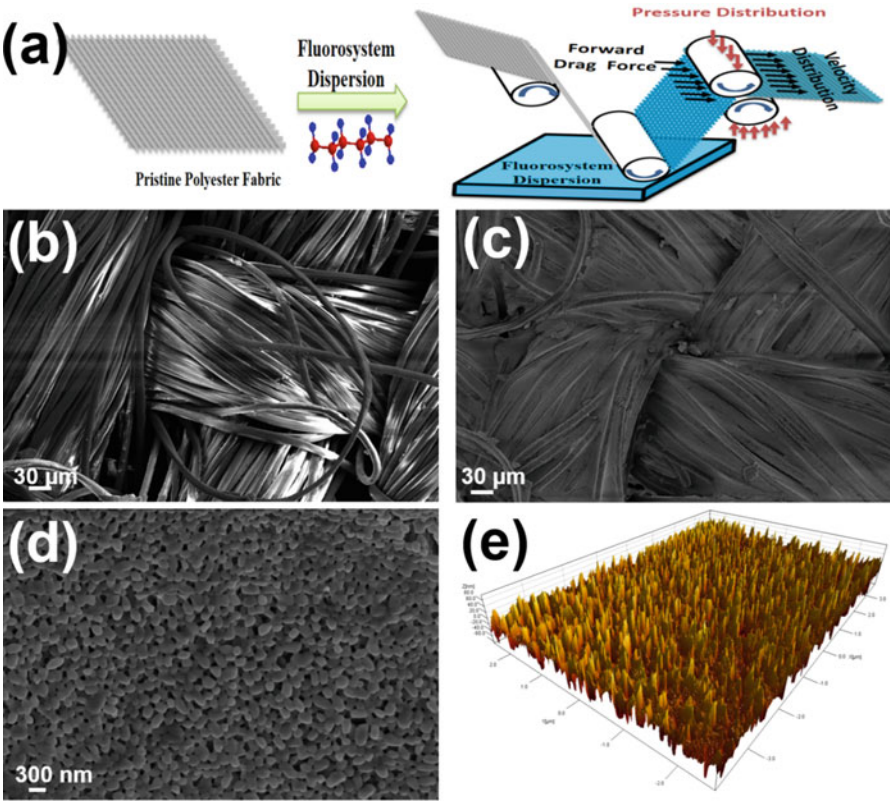

Fig. 14.9 (**a**) Padding Process, FE-SEM micrograph of (**b**) pristine polyester fabric, and (**c**) dispersion-coated fabric, (**d**) FE-SEM micrograph of dispersion-coated fabric at 300 nm scale, (**e**) simulated 3D projection of FE-SEM micrograph

squeezing rollers removes excess quantity of dispersion from the fabric, whereas the forward drag force ensures the uniform velocity distribution during padding (Birley et al. 1992; Makowski et al. 2016) (Fig. 14.9a, b). Therefore, the synergistic effect of these two parameters helps in maintaining the constant thickness, i.e., 30 µm, and controls the shrinkage and stretch growth in the coated Janus fabric (Birley et al. 1992; Makowski et al. 2016; Sarwar et al. 2017).

Polyester fabric samples of dimension 12 × 12 cm^2 were cleaned with Acetone for 20 min and then with DI water for 15 min in an ultrasonic bath (20 kHz frequency) for removing any traces of impurities. After coating fluorosystem dispersion onto the cleaned polyester fabric, it was kept at room temperature for 2 h. Then, the coated fabric was passed in an air-oven at 150 °C for 6 h for the complete removal of water phase and wetting agent from the dispersion (Chemours 2016). The engineered Janus fabric showed a thickness of 30 µm (measured by digital thickness gauge meter), then the fabric samples were taken for further characterizations.

The morphology of the fabric was analyzed via Field Emission Scanning Electron Microscope (Carl-Zeiss AG, JSM-6700F, Germany) with 3 kV accelerating voltage. The wetting study was done using static contact angle goniometer (DSA100, Krüss GmbH, Germany) using DI water (8 μL volume) at room temperature. The water contact angles (WCA) were measured after resting the droplet on the surface for 2 s, then the average of five reading was taken. The anti-icing study was performed by sprinkling DI water droplets of 20 μL volume (cooled at −5 °C) using a micropipette (Tarsons 2–20 μL (microliter) T20 Accupipette) on the pre-cooled surface of Janus fabric samples, which were subsequently placed in a NEWTRONIC deep-freezer system for 15 min (at −20 °C) to get the frozen droplets. Then, the pressurized airstream was progressively passed on the fabric samples at an approximate rate of 10 kPa/s via air-compressor until the frozen water droplets detached and rolled-off. The distance between the air gun and Janus fabric was maintained at 30 cm. The abrasion resistance study was done using a wear test machine (Pin-On-Disc Friction and Wear Test Rig, Magnum Engineers, India). The tensile testing of the fabric samples was done using a customized tensile test machine (Load capacity = 50 N, specimen dimension = 5 × 3 mm). The FT-IR study was done using a Perkin-Elmer Spectrum BX FTIR system (Perkin-Elmer Inc., USA) at room temperature in the range 4000–600 cm^{-1}.

14.5.1 Results and Discussion

The FE-SEM micrograph of pristine polyester fabric depicted in Fig. 14.9a indicates the smooth surface morphology of the weaved microfibers having average diameter of 7 μm (calculated via ImageJ software). Figure 14.9b shows the surface of the coated polyester fabric, where, after the addition of dispersion narrowly spaced randomly oriented Nano-needles (average diameter 220 nm, calculated via ImageJ software) forest like morphology is observed on the microfibers of fabric as depicted in Fig. 14.9d, e (Qi et al. 2002; Zhang and Seeger 2011; Wu et al. 2014).

A hierarchical surface morphology with closely spaced Nano-needles observed in Fig. 14.9d has been simulated three-dimensionally via Scanning Probe Image Processor software (SPIP, Image Metrology) as shown in Fig. 14.9e. Three-dimensional simulation reveals convex-shaped Nano-needles with rough surface texture, which is essentially required in superhydrophobic surfaces (Cheng et al. 2010; Sahoo and Kandasubramanian 2014b; Sahoo et al. 2015). The hierarchical surface morphology (Fig. 14.9d, e) of Janus fabric resembles the surface-texture on the wings of *Chremistica maculata,* i.e., Cicada insect, which has non-wetting property to protect itself in living environment from rain/water sources (Sun et al. 2009; Darmanin and Guittard 2015). The analytical comparison of the SEM micrographs and simulated surface of the Janus fabric revealed analogous multi-scaled hierarchical morphology on both surfaces, demonstrating successful bio-mimicking of hydrophobic Cicada wings. The bio-mimicked hierarchical surface of Janus fabric

exhibited superhydrophobic-superoleophilic nature, low ice-adhesion and self-cleaning ability.

After passing the Fluorosystem dispersion-coated Janus fabric in an air-oven at 150 °C for 6 h, the water phase and wetting agent evaporate and the Janus fabric undergoes thermal transition by exhibiting superhydrophobicity.

Superhydrophobicity in Janus fabric could be attributed to chemical interactions between low surface energy fluoro molecules/particles, i.e., —CF_2— and —CF_3, and Polyester end groups, i.e., —COOH and —OH. The Fluoro molecules in the form of —CF_2— and —CF_3 present in Fluorosystem dispersion are able to migrate to the surface of the Polyester fabric at low temperature conditions, where the macromolecules of polymer are practically immiscible and compete for surface exposure. The polar end groups, i.e., "—COOH" and "—OH," present in Polyester groups, are capable of forming Hydrogen bonding, which possibly interact with —CF_2 and —CF_3 molecules at a thermal transition temperature of 150 °C, where surfactants and stabilizing agents get evaporated (Lebold et al. 2000; Qi et al. 2002; Demir et al. 2017). This thermal transition temperature helps in promoting the migration of Fluoro particles/molecules to migrate to the surface of the Polyester fabric, where they interact with polar —COOH and —OH end groups via Hydrogen bonding, thereby decreasing the surface energy and imparting superhydrophobicity in the Fluorosystem-coated polyester fabric (Smith 1980; Lebold et al. 2000; Qi et al. 2002; Demir et al. 2017).

FT-IR characterization of fabric samples revealed small peak at 2866 and 1341 cm^{-1} corresponds to stretching of —C—H— bond in methylene groups, whereas peaks at 714 and 875 cm^{-1} correspond to in-ring bond stretching of —C—H— groups, present in ester linkage of polyester chain (Cecen et al. 2008; Parvinzadeh and Ebrahimi 2011). The characteristic peak at 1706 cm^{-1} belongs to —C—O— bond stretching of ester group in polyester, whereas other distinct peaks at 1239, 1079, and 1009 cm^{-1} correspond to —C—O— bond stretching of ester group (Parvinzadeh and Ebrahimi 2011). The small peak at 1402 cm^{-1} corresponds to —C—C— bond stretch present in aromatic ring (Cecen et al. 2008; Parvinzadeh and Ebrahimi 2011). The characteristic peaks at 1217 and 1149 cm^{-1} correspond to —C—F— bond stretching, and the small peak at 631 cm^{-1} corresponds to wagging of —F—C—F— bond, i.e., to and fro motions in CF_2 group, present in Fluorosystem (Huang et al. 2011; Zhang and Seeger 2011).

14.5.2 Wetting Behavior of Janus Fabric

The wetting behavior of Janus fabric was extensively studied using water and oils/solvents. The superhydrophobic nature attained at 150 °C in Janus fabric is accredited to the evaporation of water phase from the dispersion (Chemours 2016). However, the improvement in superhydrophobic nature from 120 to 150 °C may be attributed to the increase in surface protuberance height leading to elevated surface roughness as demonstrated by Sahoo et al. (Sahoo and Kandasubramanian

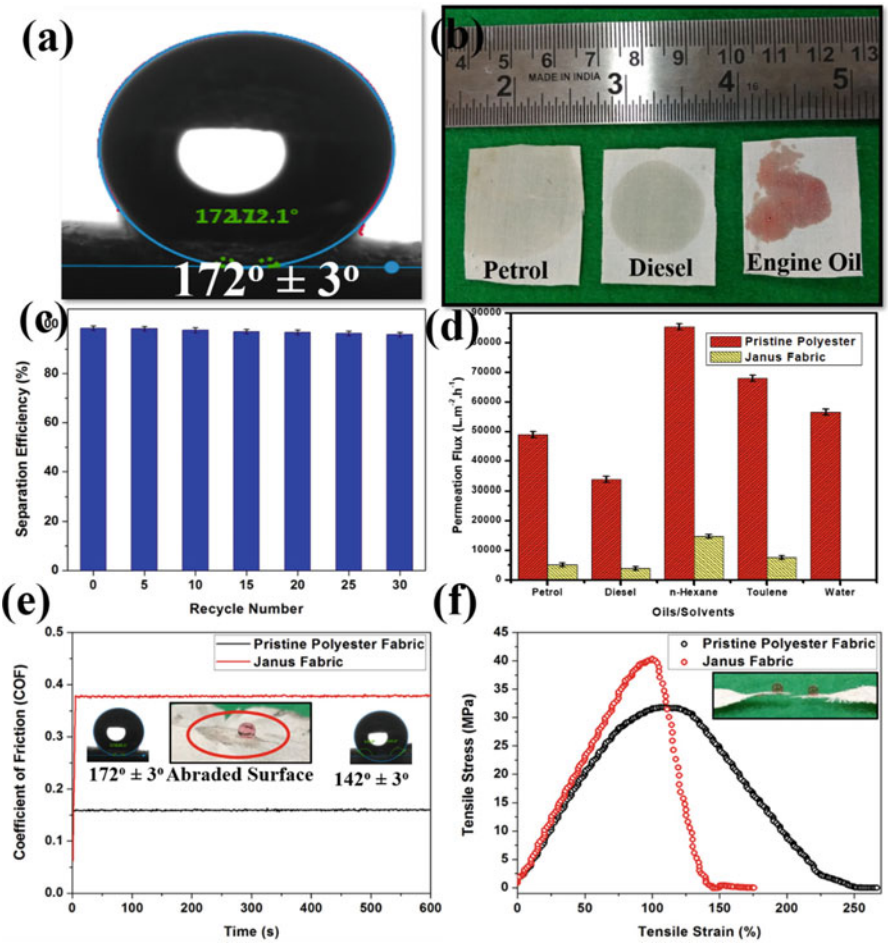

Fig. 14.10 (**a**) Superhydrophobicity of Janus fabric, (**b**) Wettability of Janus fabric, (**c**) Separation efficiency, (**d**) Permeation flux analysis, (**e**) Coefficient of friction, (**f**) Tensile strength of Janus fabric

2014b; Sahoo et al. 2015). The Janus fabric did not show enhancement in water contact angle (WCA) after 150 °C; however, beyond a heat treatment of 280 °C, polyester fabric starts losing its intrinsic property. The maximum WCA achieved was 172° ± 3° at a heat treatment of 150 °C (Fig. 14.10a).

Various wetting theories have been proposed for describing the wettability of surfaces, but Wenzel and Cassie-Baxter are widely considered for explaining the superhydrophobicity in surfaces (Wenzel 1936; Cassie and Baxter 1944; Sahoo and Kandasubramanian 2014b; Sahoo and Balasubramanian 2014; Sahoo et al. 2015; Gupta and Kandasubramanian 2017a). According to Wenzel's theory, the roughness in homogeneous surface is main driving factor for improving the hydrophobicity,

which is explained in previous section (Wenzel 1936; Sahoo and Kandasubramanian 2014b; Gore and Kandasubramanian 2018).

Cassie-Baxter's theory explained the superhydrophobicity of a heterogeneous rough surfaced Janus fabric having porosity, and it is given by equation mentioned in previous section (Sahoo and Kandasubramanian 2014b; Arora and Balasubramanian 2014; Sahoo et al. 2015; Gupta and Kandasubramanian 2017a). The Cassie-Baxter's regime has a porosity on its surface which entraps the air in between liquid and solid phase, thereby creating small air-pockets; this subsequently leads to the enhancement in hydrophobic nature of the surface (Cassie and Baxter 1944; Sahoo and Kandasubramanian 2014b; Sahoo et al. 2015; Gupta and Kandasubramanian 2017a; Gore and Kandasubramanian 2018). Sahoo et al. have reported that elevation in WCA of a superhydrophobic surface mainly depends on the Cassie-Baxter's model, where the porous structure and roughness are the main contributing features, which leads to the formation of air-pockets, thereby reducing the adhesion between liquid and solid phase (Sahoo and Kandasubramanian 2014b; Sahoo and Balasubramanian 2014; Sahoo et al. 2015).

Superhydrophobic surface possesses self-cleaning ability as demonstrated by the "Lotus effect," where a space between hierarchical structure (in our case convex-shaped Nano-needles) and surface is filled by air bubbles, thereby facilitating the water droplet to easily roll-off, which takes away any contaminant particles present on the surface along with them leading to a "self-cleaning action" (Bhushan et al. 2009; Fernández et al. 2017). The self-cleaning ability of developed Janus fabric has been demonstrated in a movie.

The Janus fabric revealed superoleophilicity, i.e., WCA ~ 0°, for various petroleum products (petrol, diesel, and engine oil) and organic solvents as shown in Fig. 14.10b. This superoleophilic nature of Janus fabric is attributed to the synergistic effect of low surface energy (imparted by fluorosystem) and hierarchical multi-scaled texture (Burkarter et al. 2007). The surface tensions of petrol ($\gamma_p = 29$ mN/m), engine oil ($\gamma_e = 65$ mN/m), and diesel ($\gamma_p = 29.5$ mN/m) are lower than water ($\gamma_w = 72.8$ mN/m), and therefore they get easily absorbed on the surface of Janus fabric. The large difference in surface tension between water and oil imparts the superhydrophobic and superoleophilic nature to the Janus fabric at room temperature, which can be utilized for oil-water separation (Zhou et al. 2013; Wang et al. 2015d; Gu et al. 2017; Gore and Kandasubramanian 2018).

Superhydrophobic material should be able to withstand an extreme environmental conditions like subzero temperature (0 to −20 °C), saline water, UV-irradiation, thermal stability, and chemical durability; considering this, the wettability of developed Janus fabric was comprehensively investigated under abovementioned environmental conditions.

Wettability of Janus fabric was evaluated in hypersaline, i.e., Sodium Chloride, solution for different concentrations from 10 to 40%. Study shows that Janus fabric maintains its superhydrophobicity till 30% saline concentration with a WCA of 152° ± 3°, but slightly decreases to 148° ± 3° in 40% saline concentration, which is attributed to the increased ionic nature of saline solution at higher concentration leading to reduction in surface tension of solid/liquid phase (Serrano-Saldaña et al.

2004). The study demonstrates that the engineered Janus fabric maintains superhydrophobicity in hypersaline solution from 0 to 30% concentrations.

The wetting behavior of Janus fabric was studied for various subzero temperatures ranging from −20 to 0 °C, where it showed a decrease in WCA with decreasing temperature. The WCAs measured were 165° at 0 °C and 139° at −20 °C; this reduction in hydrophobicity could be ascribed to the transition from Cassie-Baxter state at 0 °C to Wenzel state at −20 °C. This transition might take place due to the synergistic effect of reduced temperature and condensed water phase in the space between nano-needles and rough surface of Janus fabric (Dorrer and Rühe 2007; Sahoo et al. 2015; Gupta and Kandasubramanian 2017a; Gore and Kandasubramanian 2018).

The Janus fabric possessing frozen water droplets on its surface was bombarded with a pressurized airstream at a progressively increasing rate of 10 kPa/s, the droplets started to roll off after 5 s and detached within 8 s, after reaching an air pressure of 90 kPa. The anti-icing property of Janus fabric has been shown in movie.

The Janus fabric was bombarded with UV-irradiation of 254 nm wavelength for 72 h, which showed reduction in WCA from 172° ± 3° to 162° ± 3°, still maintaining superhydrophobic nature. The superhydrophobic performance of Janus fabric under UV-irradiation could be attributed to the presence of fluorosystem possessing a stable C—F— bond which has very short bond length of 1.35 Å and a bond energy of 504 kJ/mole (Xiu et al. 2008; Zhang and Seeger 2011; Wu et al. 2014; Lim 2016).

The chemical durability Janus fabric was investigated for establishing its robustness in strong acidic and alkaline conditions. In this study, the developed Janus fabric was immersed into the acidic (pH = 1) and alkaline (pH = 14) solutions for 72 h. The Janus fabric being exposed to strong corrosive environment showed some deterioration in WCA, but still maintained its superhydrophobicity. As mentioned earlier, the stability of the Janus fabric could be attributed to the presence of fluorosystem which contains a stable —C—F— bond which is also linked to its chemical resistance (Xiu et al. 2008; Zhang and Seeger 2011; Wu et al. 2014). The decrease in WCA could be ascribed to the oxidation/degradation in polyester polymer which has low chemical resistance against highly acidic (pH = 1) and alkaline (pH = 14) solutions (Buxbaum 1968). The significant reduction of WCA in alkaline environment might be associated with the release of Terephthalic Acid and Ethylene Glycol due to the oxidation/degradation in polyester, which is also evidenced by the discoloration in Janus fabric (Buxbaum 1968; Brueckner et al. 2008). Considering, the abovementioned studies, the Janus fabric has demonstrated a stable performance under various extreme environmental conditions.

14.5.3 Absorption Study

In order to establish the potential of Janus fabric for oil/water separation, the oil absorption study was performed. The Janus fabric efficiently absorbed and separated

Diesel from a dyed water within 2 s, without any staining. The Janus fabric demonstrated high absorption capacity of 1.5 (wt/wt) for engine oil within 15 s. The absorption capacity of Janus fabric with Diesel and Petrol was 0.8 (wt/wt) and 0.7 (wt/wt), respectively, the absorption time for both oils was 2 s. The organic solvents used in the study were n-hexane and Toluene for which the absorption capacities were 0.4 (wt/wt) and 0.6 (wt/wt), respectively, with an absorption time of 2 s each. The absorption capacity of Janus fabric was calculated by following equation (Bastani et al. 2006; Mishra and Balasubramanian 2014; Arora and Balasubramanian 2014; Gupta and Kandasubramanian 2017a; Gore and Kandasubramanian 2018):

$$\text{Absorption Capacity} = \frac{W_2 - W_1}{W_1} \tag{14.10}$$

where W_1 = weight of fabric before immersion, W_2 = weight of fabric after absorption.

The recycling ability and durability of Janus fabric are the main factors for considering practical application in oil-water separation, which was evaluated by the number of washing cycles and absorption/combustion cycles. After each absorption cycle, the oily Janus fabric was rinsed as per the standard procedure mentioned in previous section, and further the cleaned Janus fabric was dried in an air heating oven at 150 °C for 30 min to retain its superhydrophobicity. The Janus fabric demonstrated absorption capacity of 0.8 (wt/wt) for diesel till 30 washing cycles, demonstrating robustness for continuous oil-water separation. The same Janus fabric was evaluated for its superhydrophobicity after every five absorption cycles. The Janus fabric effectively retained its superhydrophobicity till 30 washing cycles with WCA from 172° ± 3° to 160° ± 3°. Similar oil absorption capacities were also investigated for Petrol, Engine oil, and organic solvents (Fig. 14.10b).

The absorption capacity was also evaluated for flame tested Janus fabric, where it showed a linear decreasing trend from 0.8 (wt/wt) to 0.1 (wt/wt) till 10 absorption cycles. The same combusted Janus fabric exhibited superhydrophobicity till 10 absorption cycles with WCA from 172° ± 3° to 150° ± 3°.

The ability of Janus fabric to retain superhydrophobicity even after burning is attributed to the presence of Fluorosystem (Huang et al. 2011; Zhang and Seeger 2011; Chemours 2016; Drobny 2016; Lim 2016). The absorption kinetic study of all the petroleum oils and organic solvents absorbed by the Janus fabric can be done by Fractal Like-Linear Driving Force model (FL-LDF) (Mishra and Balasubramanian 2014; Khosravi and Azizian 2017):

$$\ln\left(1 - \frac{m_t}{m_{\max}}\right) = -D' t^{\alpha} \tag{14.11}$$

where m_t = Mass of Oil absorbed by the Janus Fabric at time t,

$m_{\max}$ = Maximum Oil absorption capacity of Janus Fabric per unit mass,

D' = Mass transfer coefficient, (proportional to the diffusion coefficient of oil diffusion into pores, i.e., in terms of pore size and oil viscosity,

t = Absorption time, and,

α = constant, (denotes different pores with different sizes present in fabric.

14.5.4 Separation Analysis

The potency of Janus fabric as an oil-absorbing material has been investigated via oil-water separation study (Pan et al. 2008). The separation efficiency of Janus fabric was studied for various oils/solvents with water (ratio of 1:1). The oil-water mixture was poured on Janus fabric, where only oil passed through the Janus fabric to container and the water was retained on the surface, due to the difference in the surface tensions of oil/water and Janus fabric (Pan et al. 2008; Sahoo and Kandasubramanian 2014b; Xue et al. 2014; Ma et al. 2016; Gupta and Kandasubramanian 2017a; Gore and Kandasubramanian 2018).

The separation cycles were repeated for 30 times as shown in Fig. 14.10c, where the Janus fabric maintained the separation efficiency more than 95% for all washing cycles. The stability of Janus fabric was evaluated by measuring WCA after every five washing cycles as depicted in Fig. 14.10c. The Janus fabric retained superhydrophobicity within $172^\circ \pm 3^\circ$ to $165^\circ \pm 3^\circ$ till 30 washing cycles. Similar separation efficiencies were also investigated for Petrol and Engine oil (Fig. 14.10b).

The directional movement of fluid through the capillary channels of fabric or membrane are principally governed by the porosity and surface characteristic (Gu et al. 2017). Therefore, the breakthrough pressure for the engineered Janus fabric for possible penetration of water through its cross-section can be calculated by considering the fabric as an interwoven mesh with predominant cylindrical texture as described in previous section (Tuteja et al. 2008a, 2008b; Choi et al. 2009; Chhatre et al. 2010; Tian et al. 2014; Mates et al. 2014; Song et al. 2014).

The polyester fabric used in the study exhibited an average radius of cylinders 105 μm and an average inter-cylinder spacing of 275 μm as calculated from FE-SEM micrograph (Fig. 14.9b) using ImageJ software.

The petrol, engine oil, and diesel spontaneously pass through the Janus fabric owing to the difference in their surface tensions ($\gamma_{\text{Janus fabric}} > \gamma_{\text{oil}}$), but, for water ($\gamma_{\text{Janus fabric}} < \gamma_{\text{water}}$) to pass through the Janus fabric needs to cross the breakthrough pressure of 1.33 kPa, which has been calculated from Eq. (14.11). Similar results were reported by Zhou et al., where the breakthrough pressure for water was theoretically calculated and compared with experimental results (Zhou et al. 2013; Wang et al. 2015d).

14.5.5 Permeation Flux Analysis

The permeation flux study of Oils and Solvents is important for establishing its permeation rate. Therefore, the permeation flux study was performed on Petrol, Diesel, *n*-Hexane, Toluene, and Water for Janus fabric and Pristine Polyester samples. Previously described equation was used for calculating permeation fluxes (Gu et al. 2017; Liu et al. 2017; Yu et al. 2017b; Gore and Kandasubramanian 2018).

The results (Fig. 14.10d) demonstrated that *n*-Hexane solvent exhibited highest permeation flux for Pristine, i.e., 85277.46 $L{\cdot}m^{-2}{\cdot}h^{-1}$, Janus fabric, i.e., 14597.65 $L{\cdot}m^{-2}{\cdot}h^{-1}$, due to its low surface tension, as compared to other used oils and solvents. Petrol and Toluene have demonstrated permeation fluxes around 48892.41 $L{\cdot}m^{-2}{\cdot}h^{-1}$ and 67906.12 $L{\cdot}m^{-2}{\cdot}h^{-1}$ for Pristine Polyester and 5016.87 $L{\cdot}m^{-2}{\cdot}h^{-1}$ and 7501.904 $L{\cdot}m^{-2}{\cdot}h^{-1}$ for Janus fabric, respectively. Diesel has showed a permeation flux of around 33641.57 $L{\cdot}m^{-2}{\cdot}h^{-1}$ and 3771.011 $L{\cdot}m^{-2}{\cdot}h^{-1}$ for Pristine Polyester and Janus Fabric, respectively. As observed from the permeation flux results, only Pristine Polyester fabric allowed the Water to percolate and pass through its cross-sectional area, whereas the Janus fabric restricted the percolation, and thus the permeation of Water through it, due to superhydrophobic nature, i.e., WCA ~ 172°. The noticeable low permeation flux of oils and solvents for Janus fabric could be attributed to the strong adhesive and capillary forces coupled with acting surface tension arising due to action of interacting Fluoro molecules (Qi et al. 2002; Wang et al. 2015a, c; Brown and Bhushan 2015; Ma et al. 2016, 2017; Yu et al. 2017b). The high permeation rate of Pristine Polyester could be attributed to availability of unfilled pores (Fig. 14.9b), thereby allowing the easy transportation of oils and solvents; however, these pores get filled-up after coating with Fluorosystem dispersion as shown in Fig. 14.9c. The viscosity of Engine oil was high among all oils and solvents, thereby decreasing its permeation rate; therefore, the permeation flux for Engine Oil could not be calculated.

Frictional Performance. The potency of the developed Janus Fabric for practical applications as oil-water separation material also related to its mechanical stability. The surface mechanical stability of the Janus fabric was investigated by analyzing its friction resistance and tensile strength. The friction resistance of Janus fabric was evaluated via pin on disc friction and wear test rig by sliding the fabric against Wear disc EN 31 (58–60 HRC) with a speed of 4 cm/s under 5 N load for 10 min, which corresponds to a sliding distance of 24 m. Figure 14.10e depicts the variation of coefficient of friction (COF) with sliding time for pristine polyester fabric and Janus fabric demonstrating larger COF value for Janus fabric (0.38) compared with pristine polyester fabric (0.16) suggesting enhanced friction resistance owing to the presence of mild PTFE particles on stress dissipation suggesting that the PTFE lubrication effect is not sufficient to harmonize the effect of enhanced surface roughness induced by PTFE nanoparticles (Ramalho and Miranda 2005). Although, WCA of Janus fabric reduced from 172° ± 3° to 142° ± 3° after abrasion, it still retained its

hydrophobic characteristic, indicating the robustness of the Janus fabric against mechanical forces (Ramalho and Miranda 2005; Si et al. 2015).

The effect of tensile loading on the superhydrophobicity of Janus fabric was investigated via customized strain sensing system with elongation rate of 50 μm/min. The tensile strength of the Janus fabric (40.3 MPa) is higher than pristine polyester fabric (31.8 MPa) as depicted in Fig. 14.10f and is attributed to the shear response of robust PTFE coating (Testa and Yu 1987). Although Janus fabric suffers fracture as the axial tensile stress reaches 40.3 MPa, nevertheless, the broken fabric sustains still exhibits superhydrophobicity, which concludes that mechanical stretching does not destroy the fabric surface asperities (Tang et al. 2013; Gu et al. 2017). The successive results demonstrate the mechanical stability of the Janus fabric, thereby making it a proficient candidate for marine oil-spill clean-ups (Gore et al. 2018b; Tang et al. 2013).

14.5.6 Summary

The Janus fabric demonstrated superhydrophobicity-oleophilicity, and possessed an oil-water separation efficiency of 98% for various oils/solvents, with stable repeatability (till 30 washing cycles). The Janus fabric also demonstrated self-cleaning and anti-icing characteristic, flame-retardancy, high thermal stability (180 °C), subzero temperature stability (−20 °C), and a maximum permeation fluxes for *n*-Hexane, Toluene, and Petrol, i.e., 14597.65 $L{\cdot}m^{-2}{\cdot}h^{-1}$, 5016.87 $L{\cdot}m^{-2}{\cdot}h^{-1}$, and 7501.904 $L{\cdot}m^{-2}{\cdot}h^{-1}$, respectively, for Janus fabric. The Janus fabric retained intrinsic properties in harsh environments like UV-irradiation (254 nm), hypersaline solution, and acidic-alkaline solutions (pH = 1–14). Subsequently, theoretically calculated breakthrough pressure (1.33 kPa) for water permeation through Janus fabric establishes it as a proficient oil-absorbing material for effective cleaning of massive oil-seepages.

14.6 Superwettable Sponges and Foams for Effective Oil-Water Separation

Sponges and foams are one of the readily available and economical materials exhibiting porosity and primary wetting characteristics. These materials generally absorb liquids with abundant water phase, which is attributed to the oxygen-rich groups which manifest in their structure, thus limiting their applicability mostly for the water absorption, due to lower selectivity. However, by doing the chemical modification of these materials with low surface energy materials, e.g., nanoparticles, their intrinsic properties can be tailored, i.e., superhydrophobicity/oleophilicity, for the effective utilization in the selective absorption of oils and

solvents from the oily wastewater. A wide range of methods have been reported for the fabrication of superhydrophobic fabric materials, which can also be utilized for the functionalization of the foams/sponges, e.g., dip-coating, in situ method, and block co-polymer grafting (Liang and Guo 2013; Xue et al. 2013, 2014; Mishra and Balasubramanian 2014; Arora and Balasubramanian 2014; Wang et al. 2015a; Ma et al. 2016; Yu et al. 2017a).

In one of the studies, Arora and Balasubramanian have fabricated a foam based on polyvinylidene fluoride (PVDF) and nano Silicon Carbide (nano-SiC) (5 wt%) (diameter $\geq$ 100 nm) (Arora and Balasubramanian 2014). They fabricated a foam based on the separation of the solid–liquid phases by utilizing the differential solubilities of the solvent, i.e., Dimethyl Formamide (DMF), and water (non-solvent). The developed PVDF/nano-SiC foam revealed superhydrophobicity (WCA ~ 152°) and oleophilicity (OCA ~ 0°), and further showed an absorption efficiency up to 20.5 and 21.5 times its weight, for paraffin oil and engine oil, respectively (Fig. 14.11). The superhydrophobicity and the mechanical strength of the developed PVDF/nano-SiC foam was attributed to the dispersed nano-SiC

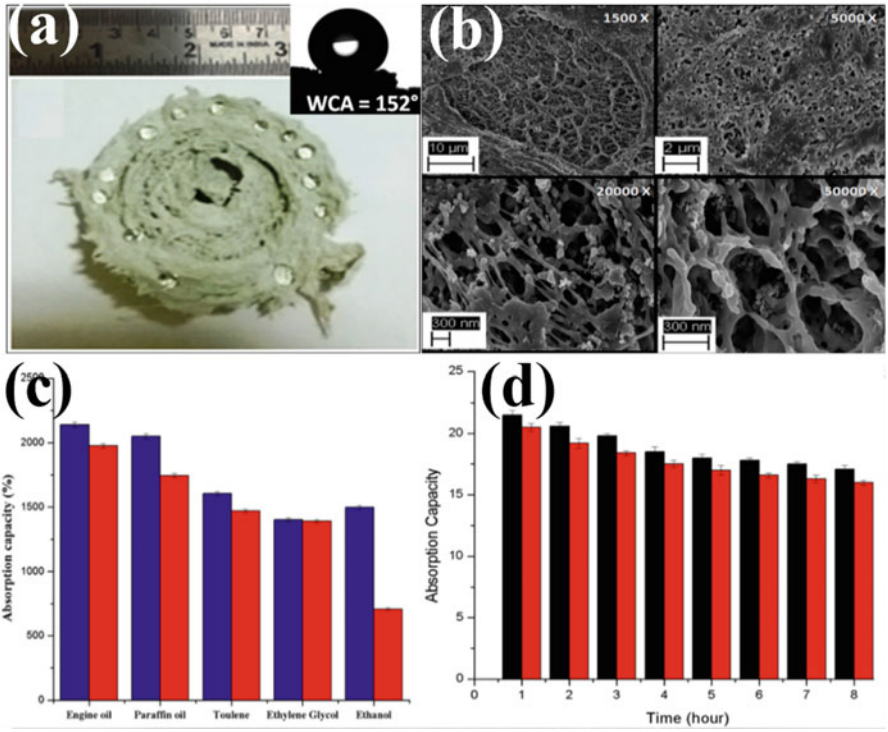

Fig. 14.11 PVDF/nano-SiC foam (**a**) Superhydrophobicity, (**b**) FESEM Analysis, (**c**) Absorption performance of oils and solvents, and (**d**) Time dependent Absorption (Arora and Balasubramanian 2014). (Reprinted with permission. Copyright 2014, Royal Society of Chemistry)

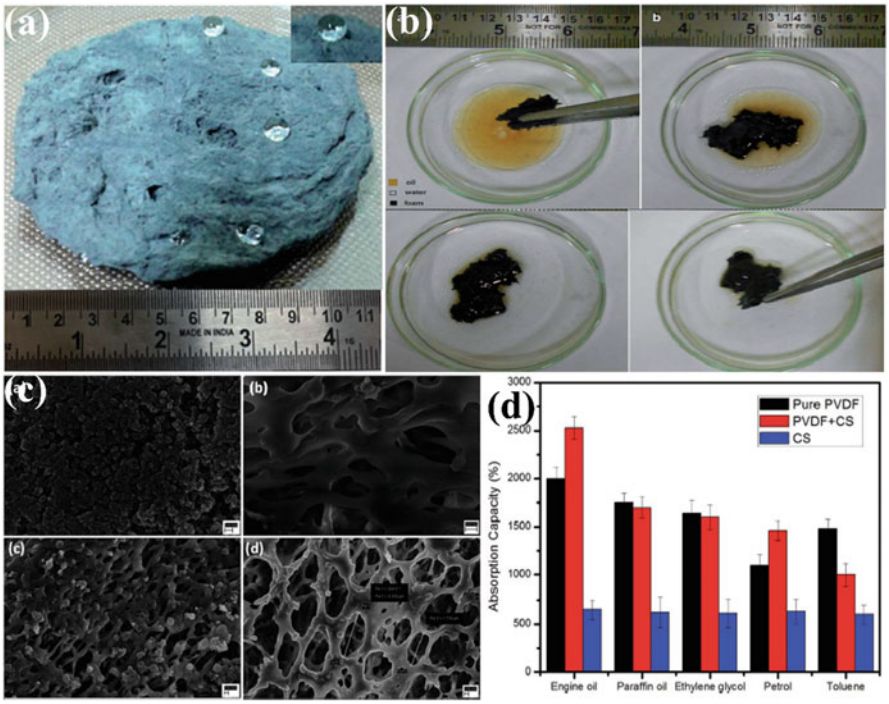

Fig. 14.12 PVDF/CS composite foam demonstrating (**a**) superhydrophobicity, (**b**) practical oil-water separation, (**c**) FESEM analysis, and (**d**) absorption performance of Camphor soot and PVDF/CS composite foam (Mishra and Balasubramanian 2014). (Reprinted with permission. Copyright 2014, Royal Society of Chemistry)

particles which exhibited the intrinsic hydrophobicity (WCA ~ 130°), and further it helped in improving the strength of the matrix (Arora and Balasubramanian 2014).

Further, the PVDF/nano-SiC foam showed reusability up to 4 cycles with mechanical squeezing, along with a minor decrease in absorption performance. They claimed that the incorporation of nano-SiC improved the mechanical strength of the foam, which helped in reducing its withering during service operation. The FESEM analysis of the PVDF/nano-SiC foam revealed a hierarchical morphology with interconnected pores in the structure, with a pore diameter varying in the range of nanometers to micrometers. Further, their FESEM analysis revealed a diversified dispersion and adhesion of the agglomerated nano-SiC nanoparticles on the periphery of the pores of the foam, thus increasing the volume of the inside pores of the foam (Arora and Balasubramanian 2014).

In another study, Mishra and Balasubramanian have fabricated a foam based on nano Camphor Soot (diameter ~ 25–60 nm) particles, and intrinsically hydrophobic PVDF polymer via non-solvent induced phase separation method (Mishra and Balasubramanian 2014). The developed PVDF/CS foam revealed superhydrophobicity (WCA ~ 170°), and superoleophilicity (OCA ~ 0°) (Fig. 14.12a, c).

The 0.5 wt % loading of CS into the PVDF/CS composite foam, improved the oil absorption capacity of up to 2500%, which was mainly attributed to the intrinsic oleophilic nature of the CS particles (Fig. 14.11b, d). The nano CS particles revealed progressively improved absorption capacity till 25 burning cycles, where it effectively absorbed the oil (Mishra and Balasubramanian 2014).

The FESEM analysis revealed a nano/-micro porous hierarchical morphology (Fig. 14.12c), which helped in enhancing oleophilicity, and simultaneously (OCA ~ 0°) improving the superhydrophobicity (WCA ~ 170°) in the PVDF/CS composite foam. They claimed that the CS particles exhibited interconnected fractal network structure of nanotubes, thus revealing a fractal-like morphology of carbon nanospheres, where 2 to 3 nanotubes emanate from the nanoparticles, and further the single nanotube help in holding 4 to 8 nanoparticle, thus forming a three-dimensional network which directly enhanced the oil absorption capacity of the PVDF/CS composite foam (Fig. 14.12c). Further, they reported that a single nanotube connects 4–8 nanoparticles, with 2–3 nanotubes growing from a single nanoparticle, thus denoting a three-dimensional network. This three-dimensional network of porous CS particles is analogous to a three-dimensional capillary network, which has a propensity for absorption, owing to capillary pressure (Mishra and Balasubramanian 2014).

In another study Li et al. have developed a melamine based sponge engineered with Copper Oxide (Cu_2O) with different crystal structures of the materials, i.e., cubic, octahedral, and cubo-octahedral, using dip-coating of Cu_2O onto melamine sponge (Fig. 14.13) (Li et al. 2018). The developed Melamine/Cu_2O Sponge demonstrated a hydrophobicity (WCA ~ 149°) and oleophilicity (OCA ~ 0°). The Density Function Theory (DFT) calculations showed a correlation between surface energy and the hydrophobicity of the developed sponge, where Cu_2O with (111) and Cu_2O with (100) crystals showed surface energies of 0.73 and 1.29 J/m^2, respectively. Further, their DFT calculations also revealed that sponge with octahedral Cu_2O (111) showed maximum hydrophobicity (WCA ~ 149°). The Melamine/Cu_2O (111) sponge showed maximum separation efficiency of 97.3% for Silicone Oil-Water separation, along with a stable absorption recycling performance till 8 cycles. The SEM analysis of the Sponge revealed a microporous morphology responsible for the enhanced separation and absorption efficacy of the oil-water mixture, along with the nano/-micro scaled dispersion of the Cu_2O particles on the surface of the foam. The FT-IR analysis of the Melamine/Cu_2O sponge showed a characteristic peak for Cu—O bond stretch at 697 cm^{-1}, and the peaks at 2275 and 2360 cm^{-1} revealed asymmetric bond stretching vibration of —NCO group present in the melamine (Li et al. 2018).

The developed Melamine/Cu_2O Sponge demonstrated a hydrophobicity (WCA ~ 149°) and oleophilicity (OCA ~ 0°). The Density Function Theory (DFT) calculations showed a correlation between surface energy and the hydrophobicity of the developed sponge, where Cu_2O with (111) and Cu_2O with (100) crystals showed surface energies of 0.73 and 1.29 J/m^2, respectively. Further, their DFT calculations also revealed that sponge with octahedral Cu_2O (111) showed maximum hydrophobicity (WCA ~ 149°). The Melamine/Cu_2O (111) sponge showed maximum separation efficiency of 97.3% for Silicone Oil-Water separation,

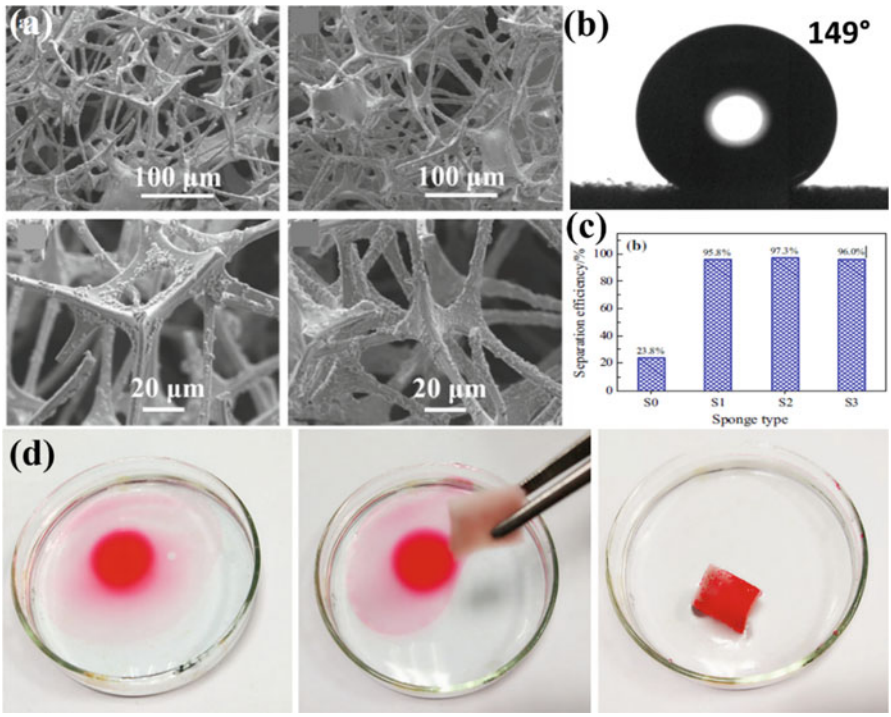

Fig. 14.13 Melamine/Cu_2O Sponge (**a**) SEM analysis, (**b**) contact angle measurement, (**c**) Separation efficiency, (**d**) Practical oil-water separation (Li et al. 2018). (Reprinted with permission. Copyright 2018, Springer Nature)

along with a stable absorption recycling performance till 8 cycles. The SEM analysis of the Sponge revealed a microporous morphology responsible for the enhanced separation and absorption efficacy of the oil-water mixture, along with the nano/-micro scaled dispersion of the Cu_2O particles on the surface of the foam (Fig. 14.13). The FT-IR analysis of the Melamine/Cu_2O sponge showed a characteristic peak for Cu—O bond stretch at 697 cm^{-1}, and the peaks at 2275 and 2360 cm^{-1} revealed asymmetric bond stretching vibration of —NCO group present in the melamine (Li et al. 2018).

In one more study, Wang et al. (2015a-d) have fabricated foam based on single-step copolymerization technique using organic-coated three-dimensional material based on dopamine and octadecylamine (ODA) onto commercially available nickel foam. The developed foam based on nickel revealed superhydrophobicity (WCA ~ 154°) (water tilting angle ~4 ± 1°) along with superoleophilicity (OCA ~ 0°) (Fig. 14.14) (Wang et al. 2015b). The SEM analysis revealed a macroporous structure in the foam along with nano/-micro scaled protrusions of the dopamine and ODA on the foam surface. Further, the surface engineered Nickel foam exhibited permeation flux of 2823, 2337, and 1844 $L{\cdot}m^{-2}{\cdot}h^{-1}$ for Lubricating oil, motor oil, and engine oil respectively. FT-IR analysis of the developed foam

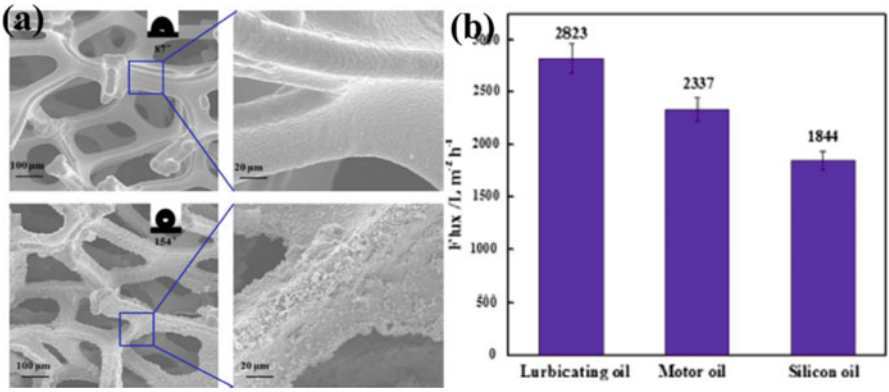

Fig. 14.14 (**a**) SEM analysis of Nickel foam, (**b**) Permeation flux analysis (Wang et al. 2015b). (Reprinted with permission. Copyright 2018, Springer Nature)

revealed peaks at 1945 and 610 cm^{-1}, which they attributed to the benzene ring present in the dopamine structure. Further, they reported peaks at 3331, 2918, and 2850 cm^{-1} associated with the stretch vibrations of the N—H, —CH_3, and —CH_2— of octadecylamine (ODA), which confirmed the copolymerization of the coated substrates onto the surface engineered foam. The developed Nickel foam exhibited ten absorption cycles, and still maintained hydrophobicity, i.e., WCA $> 142°$ (Wang et al. 2015b).

Though the Sponge and Foam based superwettable materials have been widely explored by researchers, their poor absorption performance after some usable cycles due to filling up of the pores is one of the major issues, and hence limits their applicability for long-term service applications (Mishra and Balasubramanian 2014; Arora and Balasubramanian 2014).

14.7 Conclusion and Future Direction

The contamination of oceanic and ground water sources due to oil seepages and industrial waste solvents has emerged as a global issue urging for immediate counter measures to epitomize the catastrophic repercussions on sensitive ecological system. Considering this, various superwettable materials have been explored by the researchers for the efficient oil-water separation. In this context, we have extensively discussed the nanoparticle engineered superwettable, i.e., superhydrophobic/superoleophilic, Janus materials like fabrics/textiles, membranes, electrospun nanofibers, and their practical applicability for the effective oil-water separation. Further, we have also discussed the nanoparticle decorated sponges and foams, and their pertinence for mitigating the oil-water separation challenges. In connection with superwettability of the materials, we have also explained the main driving

factors and the principle wetting theories such as Wenzel and Cassie-Baxter in the present book chapter.

Though the current research works have led to the development of highly efficient superwettable materials for practical oil-water separation, still their cost-efficiency, life cycle performance during the service period, and environment friendliness are some of the limiting factors. Considering, the rising environmental concerns, and the awareness towards the global warming, the current research focus has shifted towards developing the environment friendly, biodegradable, and robust superwettable materials for efficient oil-water separation (Sahoo and Kandasubramanian 2014b; Gore and Kandasubramanian 2018).

References

Amal Raj RB, Gonte RR, Balasubramanian K (2017) Dual functional styrene-maleic acid copolymer beads: toxic metals adsorbent and hydrogen storage. In: Enhancing cleanup of environmental pollutants. Springer International Publishing, Cham, pp 255–295

Arora R, Balasubramanian K (2014) Hierarchically porous PVDF/nano-SiC foam for distant oil-spill cleanups. RSC Adv 4:53761–53767

Arora R, Singh N, Balasubramanian K, Alegaonkar P (2014) Electroless nickel coated nano-clay for electrolytic removal of Hg(ii) ions. RSC Adv 4:50614–50623

Balasubramanian K, Sharma S, Badwe S, Banerjee B (2015) Tailored non-woven electrospun mesh of poly-Ethyleneoxide-keratin for radioactive metal ion sorption. J Green Sci Technol 2:10–19

Banerjee BS, Balasubramanian K (2015) Nanotexturing of PC/n-HA nanocomposites by innovative and advanced spray system. RSC Adv 5:13653–13659

Bastani D, Safekordi AA, Alihosseini A, Taghikhani V (2006) Study of oil sorption by expanded perlite at 298.15 K. Sep Purif Technol 52:295–300

Bhalara PD, Balasubramanian K, Banerjee BS (2015) Spider–web textured electrospun composite of graphene for sorption of Hg(II) ions. Mater Focus 4:154–163

Bhalara PD, Punetha D, Balasubramanian K (2014) A review of potential remediation techniques for uranium(VI) ion retrieval from contaminated aqueous environment. J Environ Chem Eng 2:1621–1634

Bhushan B, Jung YC, Koch K (2009) Micro-, nano- and hierarchical structures for superhydrophobicity, self-cleaning and low adhesion. Philos Trans R Soc A Math Phys Eng Sci 367:1631–1672

Birley AW, Haworth B, Batchelor J (1992) Physics of plastics: processing, properties and materials engineering. Hanser Publishers, Munich

Breitwieser M, Klingele M, Vierrath S (2018) Tailoring the membrane-electrode interface in PEM fuel cells: a review and perspective on novel engineering approaches. Adv Energy Mater 8:1701257

Brown PS, Bhushan B (2015) Mechanically durable, superoleophobic coatings prepared by layer-by-layer technique for anti-smudge and oil-water separation. Sci Rep 5:8701

Brueckner T, Eberl A, Heumann S (2008) Enzymatic and chemical hydrolysis of polyethylene terephthalate fabrics. J Polym Sci Part A Polym Chem 46:6435–6443

Brydson JA (1999) Polycarbonates. In: Plastics materials. Elsevier, Amsterdam, pp 556–583

Burkarter E, Saul CK, Thomazi F (2007) Superhydrophobic electrosprayed PTFE. Surf Coatings Technol 202:194–198

Buxbaum LH (1968) The degradation of poly(ethylene terephthalate). Angew Chemie Int Ed English 7:182–190

Cassie ABD, Baxter S (1944) Wettability of porous surfaces. Trans Faraday Soc 40:546–551

Cecen V, Seki Y, Sarikanat M, Tavman IH (2008) FTIR and SEM analysis of polyester- and epoxy-based composites manufactured by VARTM process. J Appl Polym Sci 108:2163–2170
Chemours (2016) Teflon PTFE DISP 30LX Fluoroplastic dispersion product information
Cheng Z, Gao J, Jiang L (2010) Tip geometry controls adhesive states of superhydrophobic surfaces. Langmuir 26:8233–8238
Cheng B, Li Z, Li Q, Naebe M (2017) Development of smart poly(vinylidene fluoride)-graft-poly (acrylic acid) tree-like nanofiber membrane for pH-responsive oil/water separation. J Memb Sci 534:1–8
Chhatre SS, Choi W, Tuteja A (2010) Scale dependence of omniphobic mesh surfaces. Langmuir 26:4027–4035
Choi W, Tuteja A, Chhatre S (2009) Fabrics with tunable oleophobicity. Adv Mater 21:2190–2195
Darmanin T, Guittard F (2015) Superhydrophobic and superoleophobic properties in nature. Mater Today 18:273–285
Demir T, Wei L, Nitta N (2017) Toward a long-chain Perfluoroalkyl replacement: water and oil repellency of polyethylene terephthalate (PET) films modified with Perfluoropolyether-based polyesters. ACS Appl Mater Interfaces 9:24318–24330
Dhanshetty M, Balasubramanian K (2016) Seamless coupled breathable nanocomposite Janus. In: Proceedings of 50th IRF International Conference, Pune, pp 5–10
Dorrer C, Rühe J (2007) Condensation and wetting transitions on microstructured ultrahydrophobic surfaces. Langmuir 23:3820–3824
Drobny JG (2016) Fluorine-containing polymers. In: Brydson's plastics materials: eighth edition. Elsevier, Oxford, pp 389–425
Dybal J, Schmidt P, Baldrian J, Kratochvíl J (1998) Ordered structures in polycarbonate studied by infrared and Raman spectroscopy, wide-angle X-ray scattering, and differential scanning calorimetry. Macromolecules 31:6611–6619
Fernández A, Francone A, Thamdrup LH (2017) Design of hierarchical surfaces for tuning wetting characteristics. ACS Appl Mater Interfaces 9:7701–7709
Fingas M (2012) The basics of oil spill cleanup, 3rd edn. CRC Press, Boca Raton, FL
Fingas M (2015) Handbook of oil spill science and technology. John Wiley & Sons, New York
Georgiev A, Karamancheva I, Dimov D (2008) FTIR study of the structures of vapor deposited PMDA-ODA film in presence of copper phthalocyanine. J Mol Struct 888:214–223
Ghorbel E, Hadriche I, Casalino G, Masmoudi N (2014) Characterization of thermo-mechanical and fracture behaviors of thermoplastic polymers. Materials (Basel) 7:375–398
Gonte R, Balasubramanian K (2016) Heavy and toxic metal uptake by mesoporous hypercrosslinked SMA beads: isotherms and kinetics. J Saudi Chem Soc 20:S579–S590
Gonte RR, Shelar G, Balasubramanian K (2014) Polymer–agro-waste composites for removal of Congo red dye from wastewater: adsorption isotherms and kinetics. Desalin Water Treat 52:7797–7811
Gore PM, Dhanshetty M, Kandasubramanian B (2016a) Bionic creation of nano-engineered Janus fabric for selective oil/organic solvent absorption. RSC Adv 6:111250–111260
Gore PM, Kandasubramanian B (2018) Heterogeneous wettable cotton based superhydrophobic Janus biofabric engineered with PLA/functionalized-organoclay microfibers for efficient oil-water separation. J Mater Chem A 6:7457–7479
Gore P, Khraisheh M, Kandasubramanian B (2018a) Nanofibers of resorcinol–formaldehyde for effective adsorption of As (III) ions from mimicked effluents. Environ Sci Pollut Res 25:11729–11745
Gore PM, Khurana L, Dixit R, Balasubramanian K (2017) Keratin-Nylon 6 engineered microbeads for adsorption of Th (IV) ions from liquid effluents. J Environ Chem Eng 5:5655–5667
Gore PM, Khurana L, Siddique S (2018b) Ion-imprinted electrospun nanofibers of chitosan/1-butyl-3-methylimidazolium tetrafluoroborate for the dynamic expulsion of thorium (IV) ions from mimicked effluents. Environ Sci Pollut Res 25:3320–3334

Gore PM, Zachariah S, Gupta P, Balasubramanian K (2016b) Multifunctional nano-engineered and bio-mimicking smart superhydrophobic reticulated ABS/fumed silica composite thin films with heat-sinking applications. RSC Adv 6:105180–105191

Gu J, Xiao P, Chen P (2017) Functionalization of biodegradable PLA nonwoven fabric as Superoleophilic and Superhydrophobic material for efficient oil absorption and oil/water separation. ACS Appl Mater Interfaces 9:5968–5973

Gupta RK, Dunderdale GJ, England MW, Hozumi A (2017) Oil/water separation techniques: a review of recent progresses and future directions. J Mater Chem A 5:16025–16058

Gupta P, Kandasubramanian B (2017) Directional fluid gating by Janus membranes with heterogeneous wetting properties for selective oil-water separation. ACS Appl Mater Interfaces 9:19102–19113

Gupta P, Lapalikar V, Kundu R, Balasubramanian K (2016) Recent advances in membrane based waste water treatment technology: a review. Energy Environ Focus 5:241–267

Hansen KA (2016) Physical spill countermeasures on water-response in fast currents. In: Oil spill science and technology: second edition. Elsevier, New York, NY, pp 455–482

Homaeigohar SS, Buhr K, Ebert K (2010) Polyethersulfone electrospun nanofibrous composite membrane for liquid filtration. J Memb Sci 365:68–77

Huang Q, Xiao C, Hu X, An S (2011) Fabrication and properties of poly(tetrafluoroethylene-co-hexafluoropropylene) hollow fiber membranes. J Mater Chem 21:16510–16516

Hudlikar M, Balasubramanian K, Kodam K (2014) Towards the enhancement of antimicrobial efficacy and hydrophobization of chitosan. J Chitin Chitosan Sci 2:273–279

Hunger K (ed) (2002) Industrial dyes. Wiley-VCH Verlag GmbH & co. KGaA, Weinheim, FRG

Jiang J (ed) (2010) Functional Phthalocyanine molecular materials. Springer Berlin Heidelberg, Berlin

Kamo N, Kurosawa S (1992) Characteristics of sorption of various gases to plasma-polymerized copper Phthalocyanine. Langmuir 8:254–256

Khanale M, Balasubramanian K (2016) Molecular simulation of geometrically optimized polyoxymethylene/poly (vinylalcohol) gel membrane for electroless scrubbing Ni(II) ions. J Environ Chem Eng 4:434–439

Khosravi M, Azizian S (2017) Preparation of superhydrophobic and superoleophilic nanostructured layer on steel mesh for oil-water separation. Sep Purif Technol 172:366–373

Khurana L, Balasubramanian K (2016) Adsorption potency of imprinted starch/PVA polymers confined ionic liquid with molecular simulation framework. J Environ Chem Eng 4:2147–2154

Lebold A, Smithies A, Andrew E (2000) Fluorocarbon particle coated textiles for use in electrostatic printing machines. p 1–7

Li J, Huang ZQ, Xue C (2018) Facile preparation of novel hydrophobic sponges coated by Cu_2O with different crystal facet structure for selective oil absorption and oil/water separation. J Mater Sci 53:10025–10038

Liang W, Guo Z (2013) Stable superhydrophobic and superoleophilic soft porous materials for oil/water separation. RSC Adv 3:16469–16474

Lim HCA (2016) Thermoplastic polyesters. In: Brydson's plastics materials: eighth edition. Elsevier, Oxford, pp 527–543

Lin X, Yang M, Jeong H (2016) Durable superhydrophilic coatings formed for anti-biofouling and oil-water separation. J Memb Sci 506:22–30

Liu M, Hou Y, Li J, Guo Z (2017) Stable superwetting meshes for on-demand separation of immiscible oil/water mixtures and emulsions. Langmuir 33:3702–3710

Ma Q, Cheng H, Fane AG (2016) Recent development of advanced materials with special wettability for selective oil/water separation. Small 12:2186–2202

Ma W, Guo Z, Zhao J (2017) Polyimide/cellulose acetate core/shell electrospun fibrous membranes for oil-water separation. Sep Purif Technol 177:71–85

Makowski T, Grala M, Fortuniak W (2016) Electrical properties of hydrophobic polyester and woven fabrics with conducting 3D network of multiwall carbon nanotubes. Mater Des 90:1026–1033

Mates JE, Schutzius TM, Qin J (2014) The fluid diode: tunable unidirectional flow through porous substrates. ACS Appl Mater Interfaces 6:12837–12843
Matsubayashi T, Tenjimbayashi M, Komine M (2017) Bioinspired hydrogel-coated mesh with superhydrophilicity and underwater superoleophobicity for efficient and ultrafast oil/water separation in harsh environments. Ind Eng Chem Res 56:7080–7085
Mishra P, Balasubramanian K (2014) Nanostructured microporous polymer composite imprinted with superhydrophobic camphor soot, for emphatic oil-water separation. RSC Adv 4:53291–53296
Moser FH, Thomas AL (1964) Phthalocyanine compounds. J Chem Educ 41:245
Padaki M, Surya Murali R, Abdullah MS (2015) Membrane technology enhancement in oil-water separation. A review. Desalination 357:197–207
Padhi S, Gosavi S, Ramdayal Yadav BK (2018) Quantitative evolution of wetting phenomena for super hydrophobic surfaces. Mater Focus 7:305–315
Padma N, Joshi A, Singh A (2009) NO_2 sensors with room temperature operation and long term stability using copper phthalocyanine thin films. Sensors Actuators B Chem 143:246–252
Pan Q, Wang M, Wang H (2008) Separating small amount of water and hydrophobic solvents by novel superhydrophobic copper meshes. Appl Surf Sci 254:6002–6006
Parshin AM, Gunyakov VA, Zyryanov VY, Shabanov VF (2013) Domain structures in nematic liquid crystals on a polycarbonate surface. Int J Mol Sci 14:16303–16320
Parvinzadeh M, Ebrahimi I (2011) Influence of atmospheric-air plasma on the coating of a nonionic lubricating agent on polyester fiber. Radiat Eff Defects Solids 166:408–416
Qi H, Sui K, Ma Z et al (2002) Polymeric fluorocarbon-coated polyester substrates for waterproof breathable fabrics. Text Res J 72:93–97
Ramalho A, Miranda JC (2005) Friction and wear of electroless NiP and NiP + PTFE coatings. Wear 259:828–834
Rezaeifard A, Jafarpour M, Naeimi A, Salimi M (2012) Efficient and highly selective aqueous oxidation of alcohols and sulfides catalyzed by reusable hydrophobic copper (II) phthalocyanine. Inorg Chem Commun 15:230–234
Rule P, Balasubramanian K, Gonte RR (2014) Uranium(VI) remediation from aqueous environment using impregnated cellulose beads. J Environ Radioact 136:22–29
Sahoo BN, Balasubramanian K (2014) Facile synthesis of nano cauliflower and nano broccoli like hierarchical superhydrophobic composite coating using PVDF/carbon soot particles via gelation technique. J Colloid Interface Sci 436:111–121
Sahoo BN, Balasubramanian K, Sucheendran MM (2015) Thermally triggered transition of superhydrophobic characteristics of micro and Nano textured multiscale rough surfaces. J Phys Chem C 119(25):14201–14213
Sahoo BN, Kandasubramanian B (2014a) An experimental design for the investigation of water repellent property of candle soot particles. Mater Chem Phys 148:134–142
Sahoo BN, Kandasubramanian B (2014b) Recent progress in fabrication and characterisation of hierarchical biomimetic superhydrophobic structures. RSC Adv 4:22053–22093
Sahoo BN, Kandasubramanian B (2014c) Photoluminescent carbon soot particles derived from controlled combustion of camphor for superhydrophobic applications. RSC Adv 4:11331–11342
Sahoo BN, Kandasubramanian B, Sabarish B (2013) Controlled anisotropic wetting behaviour of multi-scale slippery surface structure of non fluoro polymer composite. Express Polym Lett 7:900–909
Sahoo BN, Sabarish B, Balasubramanian K (2014) Controlled fabrication of non-fluoro polymer composite film with hierarchically nano structured fibers. Prog Org Coatings 77:904–907
Saini S, Kandasubramanian B (2018) Engineered smart textiles and Janus microparticles for diverse functional industrial applications. Polym Plast Technol Eng:1–17. https://doi.org/10.1080/03602559.2018.1466177
Salzman RF, Xue J, Rand BP (2005) The effects of copper phthalocyanine purity on organic solar cell performance. Org Electron Phys Mater Appl 6:242–246

Sarwar N, Mohsin M, Bhatti AA (2017) Development of water and energy efficient environment friendly easy care finishing by foam coating on stretch denim fabric. J Clean Prod 154:159–166
Schwieger T, Peisert H, Golden MS (2002) Electronic structure of the organic semiconductor copper phthalocyanine and K-CuPc studied using photoemission spectroscopy. Phys Rev B 66:155207
Seoudi R, El-Bahy GS, El Sayed ZA (2005) FTIR, TGA and DC electrical conductivity studies of phthalocyanine and its complexes. J Mol Struct 753:119–126
Serrano-Saldaña E, Domínguez-Ortiz A, Pérez-Aguilar H (2004) Wettability of solid/brine/n-dodecane systems: experimental study of the effects of ionic strength and surfactant concentration. Colloids Surf A Physicochem Eng Asp 241:343–349
Sharma S, Balasubramanian K, Arora R (2016) Adsorption of arsenic (V) ions onto cellulosic-ferric oxide system: kinetics and isotherm studies. Desalin Water Treat 57:9420–9436
Shi H, He Y, Pan Y (2016) A modified mussel-inspired method to fabricate TiO_2 decorated superhydrophilic PVDF membrane for oil/water separation. J Memb Sci 506:60–70
Si Y, Fu Q, Wang X (2015) Superelastic and Superhydrophobic nanofiber-assembled cellular aerogels for effective separation of oil/water emulsions. ACS Nano 9:3791–3799
Simon S, Kandasubramanian B (2018) Facile immobilization of camphor soot on electrospun hydrophobic membrane for oil-water separation. Mater Focus 7:295–303
Simon S, Malik A, Kandasubramanian B (2018) Hierarchical electrospun super-hydrophobic nanocomposites of fluoroelastomer. Mater Focus 7:194–206
Smith C (1980) Fire retardant polyester-polytetrafluoroethylene compositions
Song J, Huang S, Lu Y (2014) Self-driven one-step oil removal from oil spill on water via selective-wettability steel mesh. ACS Appl Mater Interfaces 6:19858–19865
Sun M, Watson GS, Zheng Y (2009) Wetting properties on nanostructured surfaces of cicada wings. J Exp Biol 212:3148–3155
Tang X, Si Y, Ge J (2013) In situ polymerized superhydrophobic and superoleophilic nanofibrous membranes for gravity driven oil-water separation. Nanoscale 5:11657–11664
Testa RB, Yu LM (1987) Stress-strain relation for coated fabrics. J Eng Mech 113:1631–1646
Tian X, Li J, Wang X (2012b) Anisotropic liquid penetration arising from a cross-sectional wettability gradient. Soft Matter 8:2633–2637
Tian Y, Su B, Jiang L (2014) Interfacial material system exhibiting superwettability. Adv Mater 26:6872–6897
Tian D, Zhang X, Tian Y (2012a) Photo-induced water-oil separation based on switchable superhydrophobicity- superhydrophilicity and underwater superoleophobicity of the aligned ZnO nanorod array-coated mesh films. J Mater Chem 22:19652–19657
Tuteja A, Choi W, Mabry JM (2008a) Robust omniphobic surfaces. Proc Natl Acad Sci USA 105:18200–18205
Tuteja A, Choi W, McKinley GH (2008b) Design parameters for superhydrophobicity and superoleophobicity. MRS Bull 33:752–758
Walker AH, Scholz D, McPeek M (2018) Comparative risk assessment of spill response options for a deepwater oil well blowout: part III. Stakeholder engagement. Mar Pollut Bull 133:970. https://doi.org/10.1016/j.marpolbul.2018.05.009
Walther A, Müller AHE (2008) Janus particles. Soft Matter 4:663–668
Walther A, Müller AHE (2013) Janus particles: synthesis, self-assembly, physical properties, and applications. Chem Rev 113:5194–5261
Wang G, He Y, Wang H (2015c) A cellulose sponge with robust superhydrophilicity and under-water superoleophobicity for highly effective oil/water separation. Green Chem 17:3093–3099
Wang B, Liang W, Guo Z, Liu W (2015a) Biomimetic super-lyophobic and super-lyophilic materials applied for oil/water separation: a new strategy beyond nature. Chem Soc Rev 44:336–361
Wang E, Wang H, Liu Z (2015b) One-step fabrication of a nickel foam-based superhydrophobic and superoleophilic box for continuous oil–water separation. J Mater Sci 50:4707–4716

Wang H, Zhou H, Niu H (2015d) Dual-layer superamphiphobic/superhydrophobic-oleophilic nanofibrous membranes with unidirectional oil-transport ability and strengthened oil-water separation performance. Adv Mater Interfaces 2:1400506

Wenzel RN (1936) Resistance of solid surfaces to wetting by water. Ind Eng Chem 28:988–994

Wu L, Li L, Li B (2015) Magnetic, durable, and superhydrophobic polyurethane@Fe_3O_4@SiO_2@fluoropolymer sponges for selective oil absorption and oil/water separation. ACS Appl Mater Interfaces 7:4936–4946

Wu L, Zhang J, Li B, Wang A (2014) Mechanical- and oil-durable superhydrophobic polyester materials for selective oil absorption and oil/water separation. J Colloid Interface Sci 413:112–117

Xiu Y, Hess DW, Wong CP (2008) UV and thermally stable superhydrophobic coatings from sol-gel processing. J Colloid Interface Sci 326:465–470

Xue Z, Cao Y, Liu N (2014) Special wettable materials for oil/water separation. J Mater Chem A 2:2445–2460

Xue Z, Sun Z, Cao Y (2013) Superoleophilic and superhydrophobic biodegradable material with porous structures for oil absorption and oil-water separation. RSC Adv 3:23432–23437

Yadav R, Zachariah S, Balasubramanian K (2016) Thermally stable transparent hydrophobic bio-mimetic dual scale spherulites coating by spray deposition. Adv Sci Eng Med 8:181–187

Yu L, Hao G, Xiao L (2017a) Robust magnetic polystyrene foam for high efficiency and removal oil from water surface. Sep Purif Technol 173:121–128

Yu Z, Yun FF, Gong Z (2017b) A novel reusable superhydrophilic NiO/Ni mesh produced by a facile fabrication method for superior oil/water separation. J Mater Chem A 5:10821–10826

Zhang J, Seeger S (2011) Polyester materials with superwetting silicone nanofilaments for oil/water separation and selective oil absorption. Adv Funct Mater 21:4699–4704

Zhou H, Wang H, Niu H, Lin T (2013) Superphobicity/philicity janus fabrics with switchable, spontaneous, directional transport ability to water and oil fluids. Sci Rep 3:2964